Eur. Phys. J. B (2021) 94:164
https://doi.org/10.1140/epjb/s10051-021-00151-6

THE EUROPEAN PHYSICAL JOURNAL B

Topical Review - Computational Methods

Extended Lagrangian Born–Oppenheimer molecular dynamics: from density functional theory to charge relaxation models

Anders M. N. Niklasson[1,a]

[1] Theoretical Division, Los Alamos National Laboratory, Los Alamos, NM 87545, USA

Received 31 March 2021 / Accepted 5 July 2021 / Published online 11 August 2021

Abstract. We present a review of extended Lagrangian Born–Oppenheimer molecular dynamics and its most recent development. The molecular dynamics framework is first derived for general Hohenberg–Kohn density functional theory and it is then presented in explicit forms for thermal Hartree–Fock theory using a density matrix formalism, for self-consistent charge density functional tight-binding theory, and for general non-linear charge relaxation models that can be designed and optimized using modern machine learning methods. Our intention is to give a self-contained but brief and hopefully pedagogical presentation.

1 Introduction

Molecular dynamics (MD) simulations provide a flexible and intuitively clear way to study materials at the atomistic level. MD can be highly versatile and powerful in applications to a broad range of problems in materials science, chemistry and molecular biology [1–9]. MD simulations are often performed with interatomic potentials that have been parameterized in advance based on classical force field models that have been fitted to high-level first principles theory or experiments. These classical MD methods are highly efficient computationally and are sometime even applicable to simulations with hundreds of billions of atoms [10,11]. While classical MD simulations can be powerful in the study of large-scale materials systems [12], they typically lack a physical transparency beyond the generated atomic phase space configurations. Details of the electronic structure are missing and important features are therefore often hard or impossible to capture, for example, quantum size effects, thermal or photo excitations of the electrons, spin-polarization, bond-breaking with the associated charge transfer, drastic changes in the electronic structure such as metal-insulator transitions, the volume changes dues to electron localization, or an insight into various mechanisms such as an altered balance between the electrostatic energy and the band energy that may drive a change in the crystalline structure through a Peirls distortion, or an increased density of states at the Fermi level that may cause a spin polarization. Even if classical force field models can be tailored to mimic some of these particular effects, at least if they are anticipated and well understood, they do not have the predictive power to capture properties dominated by unexpected changes in the underlying electronic structure. Without insights into the electronic structure, an in depth understanding of the mechanisms behind a dynamical behavior are often not possible. MD simulations using only classical force fields may therefore not only miss important physical properties, but are also of limited support for our comprehension of materials at the atomistic scale. This inhibits the usefulness of classical MD simulations in the analysis, discovery and design of new materials.

The solution to these limitations with classical MD simulations may appear obvious. We simply need to derive the interatomic forces from a quantum mechanical description of the electronic structure in a quantum-based approach to MD (QMD) simulations. Unfortunately, QMD comes with an enormous computational overhead. Even if we are able to give a transparent and detailed description of the electronic structure, such as quantum-size effects, spin-polarization, excitations, and charge-transfer, we are limited to study only very small systems over short simulation times. This is a serious limitation—rendering QMD simulations useless for many real-world problems. Accessible computational processing power is continuing to increase, but this alone will have little effect on our ability to extend the applicability of QMD simulations. Sometimes, however, it is possible to reformulate the underlying physics of a problem and recast the relevant equations in a framework that is more suitable to new solvers, algorithms and with data structures that are well adapted to modern and emerging computer architectures. A dramatic acceleration of computations can then often be achieved. This interdisciplinary form of a coordinated design approach has proven to be successful throughout

[a] e-mail: amn@lanl.gov (corresponding author)

the history of scientific computing and it is a cornerstone also for the QMD methodology we will present in this review.

In this review, we will describe the computational framework of extended Lagrangian Born–Oppenheimer molecular dynamics (XL-BOMD) [13–31]. XL-BOMD was introduced to reduce the computational overhead of QMD simulations within the Born–Oppenheimer approximation. In this way the range of applications for practical QMD simulations can be extended to larger systems and longer simulation times. XL-BOMD represents only a single step in a long development of QMD methods that goes back to the early formulations of quantum mechanics. The context that initiated the development of XL-BOMD will help us better understand the new framework. Some background of QMD and the early forms of XL-BOMD will therefore be discussed as well as established QMD methods such as regular, direct Born–Oppenheimer molecular dynamics (BOMD), Ehrenfest molecular dynamics (EMD), and Car–Parrinello molecular dynamics (CPMD). This article is not a review over these well-known schemes, though the success and shortcomings of previous methods are important for the background and motivation behind the development of XL-BOMD.

XL-BOMD provides a general framework for molecular dynamics simulations that can be adapted to different levels of theory and descriptions of the electronic structure. XL-BOMD is based on an extended Lagrangian formulations, where the electronic degrees of freedom are propagated as extended dynamical variables in addition to the nuclear degrees of freedom along the molecular trajectories. Various formulations and techniques of XL-BOMD have been used in a number of software packages, including applications to density functional theory, semi-empirical electronic structure theory, polarizable force fields, excited state dynamics, and superfluidity [16,17,20,21,23,24,27,32,33,33–49]. In this way, XL-BOMD is similar to Car–Parrinello molecular dynamics (CPMD) [18,50–55], which also provides a general framework for QMD simulations based on an extended Lagrangian approach. Car–Parrinello MD was originally formulated with the extended electronic degrees of freedom expressed with plane-waves [50], but it has been used also with, for example, the charge density in orbital-free density functional theory [56–58], with the dipole moments in polarizable force-fields [59–62], with local atomic orbitals [63], the density matrix [64–66], and in combination with correlated electrons [67].

To illustrate the broad applicability of XL-BOMD it will be derived from general Hohenberg–Kohn density functional theory, which forms a theoretical basis both for orbital-free and many orbital-based electronic structure methods [30]. We will also present three explicit formulations of XL-BOMD: the first for quantum chemistry applications using a density matrix formalism based on thermal Hartree–Fock theory; the second for semi-empirical self-consistent-charge density-functional tight-binding (SCC-DFTB) theory; and the third for coarse grained charge relaxation models, where the charge-dependent interatomic potential can be parameterized, for example, with modern machine learning techniques using deep neural networks and large data sets of pre-calculated data. These examples span a broad range of possible applications across different levels of theory. However, we will not go beyond the single-particle picture of the electrons in our presentation of XL-BOMD. In contrast to CPMD, which provides a natural formulation of QMD also for the exact many-body electronic wavefunction, XL-BOMD is currently best suited for effective single-particle or mean-field descriptions of the electrons and for orbital-free charge relaxation models.

After a brief background of QMD, including established alternative methods and earlier forms of XL-BOMD, the QMD framework of XL-BOMD will be presented in its most recent form based on a general Hohenberg–Kohn density functional formulation. We then present how to integrate the equations of motion and, in particular, how the integration of the extended electronic equations of motion can be performed using a preconditioned low-rank Krylov subspace approach. A simple driven harmonic oscillator model is used to illustrate some of the particular challenges that appear in the integration of the combined nuclear and electronic degrees of freedom in XL-BOMD. We then give formulations of XL-BOMD for thermal Hartree–Fock and SCC-DFTB theory that also can be used to treat reactive degenerate systems, where the electronic gap is opening and closing along the molecular trajectories. Thereafter, we discuss more approximate, nonlinear charge relaxation models that we believe are particularly suitable for modern machine learning techniques. Each of the three formulations of XL-BOMD are demonstrated with a simple example. At the end we discuss some applications of XL-BOMD before giving a brief summary and an outlook to future challenges and opportunities.

Atomic units ($e = \hbar^2/m_e = 2\pi\epsilon_0 = 1$) are used throughout the article if not otherwise stated.

2 Quantum-based molecular dynamics

2.1 The Born–Oppenheimer approximation

In QMD the Born–Oppenheimer approximation [54,55,68,69] is of fundamental importance, because it enables practically feasible simulations by a separation of the nuclear and the electronic coordinates. In this way we can combine classical molecular dynamics with interatomic forces that are generated on-the-fly from an electronic structure that is determined by a time-independent theory.

The Born–Oppenheimer approximation can be understood from the intuitive picture that the light and fast electrons evolve on a much more rapid time scale compared to the heavier and slower nuclear degrees of freedom. We therefore assume that electrons are able to instantaneously respond to the nuclear motion and

relax to their equilibrated ground state. In this way, the electronic structure, in each instant of time, behaves as if it is in a fully relaxed stationary state that is determined by a time-independent external potential given by fixed nuclear positions. This allows a separation in the solution of the electronic wavefunctions from the nuclear degrees of freedom, where the potential energy surface is determined from the relaxed stationary state of the electrons with fixed atomic positions. The same separation is possible also when we assign a thermal distribution to the electrons, i.e. we assume that the electronic degrees of freedom undertake an instantaneous thermal equilibration for each new nuclear configuration for some predefined electronic temperature. In principle, this assumption goes beyond the traditional Born–Oppenheimer approximation, because the electrons are thermally excited and not in their ground state. However, in this article we will also use this instantaneous electronic free energy equilibration as a part of a generalized Born–Oppenheimer approximation. The thermal equilibration is of importance to degenerate systems, because at elevated electronic temperatures it introduces fractional occupation numbers that remove instabilities associated with the ground state solutions and the integer degeneracies. Apart from the generalized Born–Oppenheimer approximation we will further assume that the nuclear degrees of freedom are treated classically. However, we should not forget that the Born–Oppenheimer approximation has many limitations, though in this article it will be assumed to be valid unless otherwise stated.

It is interesting to note that the first application of the Born–Oppenheimer approximation predates its theoretical justification by Max Born and Robert Oppenheimer. Walter Heitler and Fritz London published their famous paper on the interatomic potential energy surface of the hydrogen molecule [68], which was derived for the relaxed electronic ground state with stationary nuclear positions, about half a year prior to the seminal paper by Born and Oppenheimer.

2.2 Ehrenfest molecular dynamics

A practically feasible alternative formulation for QMD simulations that does not rely on the full Born–Oppenheimer approximation is Ehrenfest MD [54]. In Ehrenfest MD the *time-dependent* Schrödinger equation is solved for the electronic degrees of freedom in each time step from which the interatomic forces for the classical nuclear degrees of freedom are determined on-the-fly for each new instantaneous electronic state. In this case the electrons never reach their relaxed ground state as the atoms are moving. However, as long as the time scales for the nuclear and electronic degrees of freedom are well separated, and the electronic degrees of freedom is in an initial ground state, the electronic wavefunction will closely follow the fully relaxed ground state solution along the molecular trajectories. If chemical reactions (with conical intersections) occur, this separation is no longer possible. A major disadvantage with Ehrenfest MD is the fast time scale of the electronic degrees of freedom, which requires very short integration time steps, and an inconsistency between the description of the time-dependent quantum mechanical electronic evolution and the classical nuclear degrees of freedom, where the electronic wavefunction may oscillate between different states while the nuclear positions just follow a single "average" classical path. In Born–Oppenheimer MD this potential inconsistency is avoided, because the electronic degrees of freedom follow a single (thermally) relaxed ground state along the molecular trajectories and the time scale is governed only by the slower nuclear motion, which allows much longer integration time steps.

2.3 Born–Oppenheimer and Car–Parrinello molecular dynamics

In regular, or direct Born–Oppenheimer molecular dynamics, the interatomic forces are calculated on-the-fly from the potential energy surface that is determined by the equilibrated stationary solution of the electrons with fixed nuclear positions in each time step, as motivated by the Born–Oppenheimer approximation. In density functional or Hartree–Fock theory this instantaneously relaxed electronic state is given as a self-consistent field (SCF) solution to a time-independent, non-linear, quantum-mechanical eigenvalue equation. The main computational obstacles in quantum-based Born–Oppenheimer MD simulations is to find this electronic ground state solution. The non-linear eigenvalue problem requires an iterative optimization procedure with repeated diagonalizations that converges to the relaxed self-consistent solution for the electrons. Because the self-consistent optimization is expensive, we usually reuse the ground state solutions from previous time steps (or some extrapolation from previous time steps) as an initial guess to the SCF optimization procedure. This drastically reduces the number of iterations required to reach convergence. However, in practice the SCF optimization is never complete and always approximate. This causes some significant problems. The extrapolation followed by an incomplete SCF optimization leads to a systematic drift in the energy, where the system is artificially heated up or cooled down. The energy drift is caused by the broken time-reversal symmetry in the underlying fictitious propagation of the electronic degrees of freedom that is generated by the extrapolation from previous time steps [13,51,70]. Only by restarting the SCF optimization from overlapping atomic charge densities, or by enforcing a very tight convergence, is it possible to avoid this problem in regular, direct Born–Oppenheimer MD. This leads to a significant increase in the computational cost.

Direct BOMD simulations were performed for molecular model systems using approximate electronic structure methods already in the early 70's by Karplus and co-workers [71,72]. These applications of BOMD were restricted to small systems and short simulations times [73] with limited impact [54]. However, a revolutionizing

breakthrough occurred in 1985, when Roberto Car and Michele Parrinello introduced an extended Lagrangian approach to first principles molecular dynamics simulations based on density functional theory [18,50–55] that avoided the non-linear eigenvalue problem and the iterative SCF optimization. Car and Parrinello molecular dynamics (CPMD) pioneered the application of practically feasible QMD simulations with true predictive power with a framework that could be used both for solids and chemical systems. With CPMD the immense scientific opportunities of MD simulations derived from ab initio theory was demonstrated for the first time. In this way CPMD opened the door to a rapid development of improved regular, direct Born–Oppenheimer MD methods [2,9,54,74,75], which followed in the late 80's and early 90's, and it also laid the ground work for XL-BOMD presented in this review.

CPMD provides a general physical framework for first principles QMD that is based on an extended Lagrangian description, where the electronic degrees of freedom are included as classical dynamical field variables that are propagated in addition to the nuclear coordinates and velocities along the molecular trajectories. The concept of an extended Lagrangian framework for MD simulations goes back to Andersen's approach to MD simulations at constant temperatures and pressures [76]. To achieve constant pressure, Andersen introduced the volume as an extended dynamical variable with a fictitious mass constant and a kinetic energy term, in addition to the nuclear coordinates, which allowed a regulation of the pressure within an isobaric ensemble. The same underlying idea was later used by Parrinello and Rahman for structural optimizations [77], where the cell shape was used a dynamical tensor variable, and later by Nose [78] for MD simulations under constant temperature or pressure. Car and Parrinello took the concept in a new direction and with a different purpose. Instead of using the extended Lagrangian to introduce some external constraints for a classical MD simulation, e.g. corresponding to the effect of an external heat bath, they included the effective single-particle electronic wavefunctions as extended classical dynamical field variables in a first-principles molecular dynamics scheme, which originally was based on Kohn–Sham density functional theory. In this way, it was possible to avoid the non-linear, quantum-mechanical, Kohn–Sham eigenvalue problem. Instead, the interatomic forces could be calculated on-the-fly from the constrained propagation of the electronic degrees of freedom with its own mass and kinetic energy. This approach may appear similar in spirit to Ehrenfest MD, but CPMD allows longer integration time steps and a control over the adiabatic separation between the electronic and nuclear degrees of freedom. In CPMD the electronic degrees of freedom are never at the exact fully relaxed self-consistent solution that defines the Born–Oppenheimer potential energy surface, but in practice they can be kept very close. Though, keep in mind that also in regular direct Born–Oppenheimer MD simulations, the electronic wavefunctions and the density are never, at least in practice, at the fully optimized and self-consistent ground state [51]. In CPMD the non-linear optimization problem is avoided and the dynamics of the extended electronic degrees of freedom is given from a physically correct time-reversible formulation instead of from an irreversible ad hoc extrapolation approach. Each force evaluation in CPMD is much faster than in regular BOMD, though a shorter integration time step is often required. The time step is determined by the size of a fictitious electron mass parameter. To ensure an adiabatic separation between the electronic and the nuclear degrees of freedom, this mass parameter needs to be kept small. This is particularly limiting for systems with a small electronic gap, where the electron mass parameter needs to be reduced. The smaller mass requires a shorter integration times steps to capture the high-frequency dynamics of a lighter electronic degrees of freedom. Another limitation with CPMD is an orthonormality condition for the electronic wavefunctions, or the corresponding idempotency condition for the density matrix. The orthonormality is enforced through a constrained dynamics, which increases the cost and can reduce the ability to achieve efficient parallelism.

2.4 Time-reversible Born–Oppenheimer molecular dynamics

So how can we avoid the shortcomings of BOMD and the limitations of CPMD? Probably the most frequently used technique for direct BOMD simulations, as mentioned above, is based on some form of extrapolation of the relaxed electron densities or wavefunctions from previous time steps that can be used as an accurate initial guess to the electronic ground state optimization for a new set of atomic positions [70,79–82]. The easiest method is to reuse the converged solution from the previous time step. Unfortunately, as discussed above, the extrapolation followed by an incomplete SCF optimization leads to the broken time-reversal symmetry in the fictitious propagation of the underlying electronic degrees of freedom, where the electrons behave as a heat source or heat sink and the system is artificially heated up or cooled down. This unphysical behavior can be avoided by introducing a perfectly time-reversible extrapolation. A time-reversible extrapolation followed by an SCF optimization is the basis for time-reversible BOMD [9,13,18,19,83,84]. Because of the time reversibility in the extrapolation of the initial guess, the iterative SCF optimization can be kept approximate without causing any systematic drift in the total energy, which provides a significant acceleration of QMD simulations.

Shortly after the introduction of time-reversible BOMD it was discovered how the method could be generated from the framework of an extended Lagrangian dynamics, where extended auxiliary electronic degrees of freedom evolved through an additional harmonic oscillator that is centered around the fully optimized Born–Oppenheimer electronic ground state solution.

The equations of motion were given in a mass zero limit of the fictitious electron mass parameter of the extend harmonic oscillator [14]. This initial formulation of XL-BOMD requires only a few SCF iterations per time step and avoids any systematic drift in the total energy that otherwise could be caused by a broken time-reversibility. However, sometimes it seemed possible to ignore the SCF optimization completely and use only a single diagonalization or density matrix construction per MD time step [15,21,34,85]. To theoretically justify this form of fully SCF-free XL-BOMD required some important modifications [22]. An approximate shadow Born–Oppenheimer potential energy surface had to be constructed and a metric tensor was introduced in the definition of the harmonic well. The equations of motion were then derived in an adiabatic limit, where, once again, the electronic mass parameter goes to zero at the same time as the frequency of the extended harmonic well goes to infinity, such that there is a clear adiabatic separation between the motion of the extended electronic degrees of freedom and the fastest nuclear motion. It is this fully SCF-free and adiabatically decoupled version of XL-BOMD [22,26,28,30] that is the main focus of this article.

3 Extended Lagrangian Born–Oppenheimer molecular dynamics

3.1 Regular direct Born–Oppenheimer molecular dynamics

In Hohenberg–Kohn density functional theory (DFT) [86–88], the Born–Oppenheimer potential energy, $U(\mathbf{R})$, for a molecular system is determined from a constrained minimization of the electronic energy functional,

$$E_{\mathrm{DFT}}[\mathbf{R},\rho] = F[\rho] + \int v_{\mathrm{ext}}(\mathbf{R},\,\mathbf{r})\rho(\mathbf{r})\mathrm{d}\mathbf{r}. \tag{1}$$

The energy functional includes a universal functional, $F[\rho]$, of the electron density, $\rho(\mathbf{r})$, and an external potential, $v_{\mathrm{ext}}(\mathbf{R},\,\mathbf{r})$, that we will assume is generated by ions at atomic position $\mathbf{R} = \{\mathbf{R}_I\}$, where $\mathbf{R}_I = [R_{Ix}, R_{Iy}, R_{Iz}]$. The constrained minimization of $E_{\mathrm{DFT}}[\mathbf{R},\rho]$ is performed over all v-representable densities, i.e. only over physically relevant densities that can be generated by electronic wavefunctions determined by some underlying potential, which integrates to the given number of electrons, N_e. The ground state density that is attained at the energy minimum (or infinum),

$$\rho_0(\mathbf{r}) = \arg\min_{\rho\in v}\left\{E_{\mathrm{DFT}}[\mathbf{R},\rho]\,\middle|\,\int\rho(\mathbf{r})\mathrm{d}\mathbf{r} = N_e\right\}, \tag{2}$$

then defines the Born–Oppenheimer potential energy,

$$U_{\mathrm{BO}}(\mathbf{R}) = F[\rho_0] + \int v_{\mathrm{ext}}(\mathbf{R},\,\mathbf{r})\rho_0(\mathbf{r})\mathrm{d}\mathbf{r} + v_{nn}(\mathbf{R}), \tag{3}$$

which also includes the repulsive ion-ion energy term, $v_{nn}(\mathbf{R})$. A Born–Oppenheimer MD can then be defined by the Lagrangian,

$$\mathcal{L}(\mathbf{R},\dot{\mathbf{R}}) = \frac{1}{2}\sum_I M_I|\dot{\mathbf{R}}_I|^2 - U_{\mathrm{BO}}(\mathbf{R}), \tag{4}$$

with the equations of motion derived from Euler–Lagrange's equations,

$$M_I\ddot{\mathbf{R}}_I = -\nabla_I U_{\mathrm{BO}}(\mathbf{R}), \tag{5}$$

and with the constant of motion,

$$E_{\mathrm{BO}}^{\mathrm{tot}} = \frac{1}{2}\sum_I M_I|\dot{\mathbf{R}}_I|^2 + U_{\mathrm{BO}}(\mathbf{R}). \tag{6}$$

The equations of motion can be integrated step by step using, for example, the frequently used velocity Verlet algorithm or other integrations schemes [8,89–96] which generate the molecular trajectories.

3.2 A shadow Born–Oppenheimer potential

The main cost in a BOMD simulation is the constrained non-linear optimization in Eq. (2), which has to be performed in each time step prior to the force evaluations. It is possible to remove the main part of this cost by replacing the non-linear universal functional, $F[\rho]$, with some approximate functional that allows a faster and easier ground state relaxation of the density. The basic idea, which is the first step in the construction of XL-BOMD, is that instead of calculating an expensive, yet still approximate ground state density, $\rho_0(\mathbf{r})$, for the exact universal functional, $F[\rho]$, by an iterative optimization procedure, we construct some approximate functional, $\mathcal{F} \approx F[\rho]$, for which we can calculate an exact ground state density, $\varrho_0(\mathbf{r})$, such that $\varrho_0(\mathbf{r}) \approx \rho_0(\mathbf{r})$, in a fast and direct way that fully avoids or significantly reduces the cost of the iterative optimization. This idea is also the principle behind backward error analysis, which has been used to construct shadow Hamiltonian methods in classical dynamics [97–99]. It is important to note that the exact form of the universal functional, $F[\rho]$, is in general unknown and that we are limited to use approximate forms such as the orbital-based Kohn–Sham functional with approximate exchange correlation terms. Small adjustments to $F[\rho]$ may therefore be irrelevant in practice. There are, of course, many possible ways to approximate the universal functional, $F[\rho]$. Maybe the most straightforward way is a linearization of $F[\rho]$ around some approximate ground state density, $n \approx \rho_0$, which gives us an approximate and n-dependent "shadow" functional,

$$\mathcal{F}[\rho,n] = F[n] + \int\left.\frac{\delta F[\rho]}{\delta\rho}\right|_{\rho=n}(\rho(\mathbf{r}) - n(\mathbf{r}))\mathrm{d}\mathbf{r}. \tag{7}$$

A more general approximation is given by an implicit definition of $\mathcal{F}[\rho,n]$, where $\mathcal{F}[\rho,n]$ is defined such that

$$F[\rho]=\mathcal{F}[\rho,n]+\mathcal{O}\left((\rho_0-n)^2\right), \tag{8}$$

which allows for mixed expansions, where some part of $F[\rho]$ can be expended to higher orders in n. This is needed in the orbital-free formulations to provide a well-defined stationary solution for the optimized electronic ground state. The approximate electronic energy density functional, replacing $E_{\mathrm{DFT}}[\mathbf{R},\rho]$ in Eq. (1), is then given by

$$\mathcal{E}_{\mathrm{DFT}}[\mathbf{R},\rho,n]=\mathcal{F}[\rho,n]+\int v_{\mathrm{ext}}(\mathbf{R},\,\mathbf{r})\rho(\mathbf{r})\mathrm{d}\mathbf{r}. \tag{9}$$

The corresponding n-dependent optimized ground state density, $\varrho_0[n](\mathbf{r})$, is attained at the lowest stationary state,

$$\varrho_0[n](\mathbf{r})=\arg\min_{\rho\in v}\left\{\mathcal{E}_{\mathrm{DFT}}[\mathbf{R},\rho,n]\,\middle|\,\int\rho(\mathbf{r})\mathrm{d}\mathbf{r}=N_e\right\}, \tag{10}$$

i.e. as the solution to

$$\frac{\delta\mathcal{E}_{\mathrm{DFT}}[\mathbf{R},\rho,n]}{\delta\rho}=0,\quad\text{where}\quad\int\rho(\mathbf{r})\mathrm{d}\mathbf{r}=N_e. \tag{11}$$

With the minimization (min) in Eq. (10) we here mean the energetically lowest stationary density given as a solution to Eq. (11). This generalization is necessary to allow $\varrho_0[n](\mathbf{r})$ to be attained also at inflection points for unbounded energy functionals. The approximate n-dependent shadow Born–Oppenheimer potential energy is then given by

$$\mathcal{U}_{\mathrm{BO}}(\mathbf{R},n)=\mathcal{F}[\varrho_0[n],n]+\int v_{\mathrm{ext}}(\mathbf{R},\mathbf{r})\varrho_0[n](\mathbf{r})\mathrm{d}\mathbf{r}+v_{nn}(\mathbf{R}). \tag{12}$$

3.3 The extended Lagrangian

The error in the shadow potential energy, $\mathcal{U}_{\mathrm{BO}}(\mathbf{R},n)$, in Eq. (12), is of second order in the residual functional, $f[n]=\varrho_0[n]-n$, i.e. the error scales as $\mathcal{O}\left(|\varrho_0[n]-n|^2\right)$. If $f[n]=0$ the variationally optimized density $\varrho_0[n]$ is the exact self-consistent solution, because the linearization of $F[\rho]$ was performed around $n=\rho_0$. Only if we can keep $n(\mathbf{r})$ close to the self-consistent exact ground state, $\rho_0(\mathbf{r})$, is the linearization accurate, which therefore also means that $n(\mathbf{r})$ should be close to $\varrho_0[n](\mathbf{r})$. We can achieve this by letting $n(\mathbf{r})$ evolve closely to the exact ground state density, $\rho_0(\mathbf{r})$, or at least a best available approximation to the ground state, as provided $\varrho_0[n](\mathbf{r})$. In XL-BOMD we accomplish this by introducing $n(\mathbf{r})$ and $\dot{n}(\mathbf{r})$ as additional classical field variables that are propagated through an extended harmonic oscillator, where the oscillations of $n(\mathbf{r})$ are centered around $\varrho_0[n](\mathbf{r})$. In a molecular dynamics simulation this harmonic oscillator will keep $n(\mathbf{r})$ close to $\varrho_0[n](\mathbf{r})$ and therefore also to $\rho_0(\mathbf{r})$. In this way we can replace the regular Born–Oppenheimer potential, $U_{\mathrm{BO}}(\mathbf{R})$, with the approximate shadow potential, $\mathcal{U}_{\mathrm{BO}}(\mathbf{R},n)$.

The extended Born–Oppenheimer Lagrangian [22,26] that is based on the shadow potential, $\mathcal{U}_{\mathrm{BO}}(\mathbf{R},n)$, and that includes $n(\mathbf{r})$ and $\dot{n}(\mathbf{r})$ as extended dynamical field variables propagated through the harmonic oscillator centered around $\varrho_0[n](\mathbf{r})$ is defined by

$$\begin{aligned}\mathcal{L}(\mathbf{R},\dot{\mathbf{R}},n,\dot{n})&=\frac{1}{2}\sum_I M_I|\dot{\mathbf{R}}_I|^2-\mathcal{U}_{\mathrm{BO}}(\mathbf{R},n)+\frac{\mu}{2}\int|\dot{n}(\mathbf{r})|^2\mathrm{d}\mathbf{r}\\&\quad-\frac{\mu\omega^2}{2}\int(\varrho_0[n](\mathbf{r})-n(\mathbf{r}))T(\mathbf{r},\mathbf{r'})(\varrho_0[n](\mathbf{r'})\\&\quad-n(\mathbf{r'}))\mathrm{d}\mathbf{r}\mathrm{d}\mathbf{r'},\end{aligned} \tag{13}$$

where μ is a fictitious electronic mass parameter and ω is the frequency of the extended harmonic oscillator. $T(\mathbf{r},\mathbf{r}')$ is a symmetric positive definite metric tensor for the harmonic well that is given by

$$T(\mathbf{r},\mathbf{r'})=\int K(\mathbf{r''},\mathbf{r})K(\mathbf{r''},\mathbf{r'})\mathrm{d}\mathbf{r''}, \tag{14}$$

for some well-chosen kernel function, $K(\mathbf{r},\mathbf{r}')$. Here we choose the kernel as the inverse of the Jacobian, $J(\mathbf{r},\mathbf{r}')$, of the residual functional, $f[n]=\varrho_0[n]-n$, i.e.

$$\begin{aligned}J(\mathbf{r},\mathbf{r'})&=\frac{\delta f[n(\mathbf{r})]}{\delta n(\mathbf{r'})}=\frac{\delta\varrho_0[n](\mathbf{r})}{\delta n(\mathbf{r}')}-\delta(\mathbf{r}-\mathbf{r'}),\\K&=J^{-1}.\end{aligned} \tag{15}$$

The kernel and the metric tensor are important in the latest formulations of XL-BOMD as they make the dynamical variable density, $n(\mathbf{r})$, oscillate around an even closer approximation to the exact Born–Oppenheimer ground state density, $\rho_0(\mathbf{r})$, than the optimized ground state, $\varrho_0[n](\mathbf{r})$, of the shadow Born–Oppenheimer potential [22,26].

3.4 Equations of motion

The equations of motion for the nuclear coordinates and the evolution of the density can be derived from Euler–Lagrange equations for the extended Lagrangian in Eq. (13), i.e.

$$\begin{aligned}\frac{\mathrm{d}}{\mathrm{d}t}\left(\frac{\partial\mathcal{L}(\mathbf{R},\dot{\mathbf{R}},n,\dot{n})}{\partial\dot{\mathbf{R}}_I}\right)&=\frac{\partial\mathcal{L}(\mathbf{R},\dot{\mathbf{R}},n,\dot{n})}{\partial\mathbf{R}_I},\\\frac{\mathrm{d}}{\mathrm{d}t}\left(\frac{\delta\mathcal{L}(\mathbf{R},\dot{\mathbf{R}},n,\dot{n})}{\delta\dot{n}}\right)&=\frac{\delta\mathcal{L}(\mathbf{R},\dot{\mathbf{R}},n,\dot{n})}{\delta n}.\end{aligned} \tag{16}$$

A straightforward derivation from the Euler–Lagrange equations leads to a fairly unpractical set of coupled equations,

$$
\begin{aligned}
M_I\ddot{\mathbf{R}}_I = &-\nabla_I \mathcal{U}_{\mathrm{BO}}(\mathbf{R},n)|_n \\
&-\nabla_I\left(\frac{\mu\omega^2}{2}\int(\varrho_0[n](\mathbf{r}) \right. \\
&\left.-n(\mathbf{r}))T(\mathbf{r},\mathbf{r'})(\varrho_0[n](\mathbf{r'})-n(\mathbf{r'}))\mathrm{d}\mathbf{r}\mathrm{d}\mathbf{r'}\right)\Big|_n \\
\ddot{n}(\mathbf{r}) = &-\omega^2\int K(\mathbf{r},\mathbf{r'})\,(\varrho_0[n](\mathbf{r'})-n(\mathbf{r'}))\,\mathrm{d}\mathbf{r'} \\
&-\frac{1}{\mu}\frac{\delta\mathcal{U}_{\mathrm{BO}}(\mathbf{R},n)}{\delta n}. \qquad (17)
\end{aligned}
$$

To avoid the direct coupling between n and $\mathbf{R}$ and the computational complexity of these equations, we assert an adiabatic separation in the limit where the harmonic oscillator frequency, ω, of the fast and light extended electronic degrees of freedom is high compared to the slower and heavier nuclear motion with a highest frequency, Ω. This can be seen as a classical analog to the Born–Oppenheimer approximation that now is applied to decouple also the extended classical electronic degrees of freedom from the nuclear motion. In general we can introduce this adiabatic approximation of Eq. (17) by letting $\omega \to \infty$ and $\mu \to 0$, while $\mu\omega =$ constant [22]. A similar adiabatic or "mass-zero" limit was used in the original formulation of XL-BOMD [14] and was recently also introduced to the equations of motion in CPMD by including the adiabatic constraints through additional Lagrange multipliers [100–102]. In the asymptotic adiabatic approximation of the equations of motion in Eq. (17) we assume a $1/\omega^2$ scaling of the residual function, i.e. $|\varrho_0[n]-n| \propto 1/\omega^2$, and that $\delta\mathcal{U}_{\mathrm{BO}}(\mathbf{R},n)/\delta n \propto (\varrho_0[n]-n)$. The $\sim(\varrho_0[n]-n)$ scaling of $\delta\mathcal{U}_{\mathrm{BO}}(\mathbf{R},n)/\delta n$ is not achieved for any choice of the shadow potential, though the scaling appears, for example, in Hartree–Fock and Kohn–Sham density functional theory if we use the linear expansion of the energy functionals around n. The relation that $|\varrho_0[n]-n| \propto 1/\omega^2$ is also non-trivial. So far we have only been able to show this behavior a posteriori in numerical simulations or for simple model systems (e.g. see Fig. 4), which will be discussed below in Sect. 3.6. Using these relations in the asymptotically adiabatic limit of Eq. (17) [22], we get the equations of motion,

$$
\begin{aligned}
M_I\ddot{\mathbf{R}}_I &= -\nabla_I \mathcal{U}_{\mathrm{BO}}(\mathbf{R},n)|_n \\
\ddot{n}(\mathbf{r}) &= -\omega^2\int K(\mathbf{r},\mathbf{r'})\,(\varrho_0[n](\mathbf{r'})-n(\mathbf{r'}))\,\mathrm{d}\mathbf{r'}, \qquad (18)
\end{aligned}
$$

with the constant of motion,

$$
E_{\mathrm{XL}}^{\mathrm{tot}} = \frac{1}{2}\sum_I M_I|\dot{\mathbf{R}}_I|^2 + \mathcal{U}_{\mathrm{BO}}(\mathbf{R},n). \qquad (19)
$$

These are the key equations that determine the molecular trajectories of XL-BOMD.

Notice, that deriving the adiabatic equations of motion in the limit when $\omega \to \infty$ and $\mu \to 0$ is different from simply setting the frequency to be $\omega = \infty$ and the mass value $\mu = 0$. For example, the equations of motion for the electronic degrees of freedom in Eq. (18) contains a term that is proportional to $|\omega^2 \times (\varrho_0[n]-n)|$, which will have a finite value even as $\omega \to \infty$, because $|\varrho_0[n]-n| \propto 1/\omega^2$. The equations of motion in Eq. (18) are simply the adiabatic approximation of Eq. (17) in the asymptotic limit of large values of ω/Ω and a small extended electron mass value μ. When the equations of motion are integrated we will always use finite values of ω, whereas the dependency on the value of μ drops out and is automatically avoided in Eq. (18). In a molecular dynamics simulation we, therefore, need to make sure that the electronic frequency, ω, is sufficiently large compared to the fastest nuclear motion frequency, Ω, such that the adiabatic separation between the electronic and the nuclear motion is valid, because this is the assumption under which we derived the equations of motion. An analogous requirement also is needed for regular direct Born–Oppenheimer MD that also assume a separation in the time scales between the nuclear and the electronic degrees of freedom in the derivation of the equations of motion in Eq. (5). As we will see below in Sect. 3.6 this adiabatic separation in XL-BOMD is system independent and it is automatically fulfilled as long as we use integration time steps of the same order as we normally would use in regular direct Born–Oppenheimer MD.

We way view the equations of motion in Eq. (18) as an alternative definition of XL-BOMD in the same way as we could define regular Born–Oppenheimer MD by Eq. (5), though that would obscure the origin and the validity of the dynamics. It would also conceal how XL-BOMD can be used as a general theoretical framework for a broad class of applications. The definition of XL-BOMD through the extended Lagrangian in Eq. (13) is therefore a more natural and transparent choice, which motivates the term "XL-BOMD" instead of the earlier term "time-reversible BOMD" [13,19].

3.5 Integrating the equations of motion

The integration of the equations on motion in Eq. (18) can be performed with a number of methods, including a coupling to thermostats both for the nuclear or the electronic degrees of freedom [24,38,41,43,103]. Regular leapfrog velocity Verlet integration as well as higher order quasi-symplectic schemes have been proposed for the integration [14,45,104,105], where additional dissipative damping terms are used to keep the electronic degrees of freedom synchronized with the evolution of the nuclear degrees of freedom and the corresponding exact Born–Oppenheimer ground state density. The dissipative terms can be seen as a weak friction that balances the accumulation of intrinsic numerical noise, for example, due to finite arithmetics, similar to a Langevin dynamics [15,16,84,106]. Rapid changes in the electronic structure may also cause energy transfer to the extended Harmonic well that needs to be cooled down. The integration method that we have used most frequently in quantum-based XL-BOMD is given by the modified hybrid leapfrog velocity Verlet algorithm,

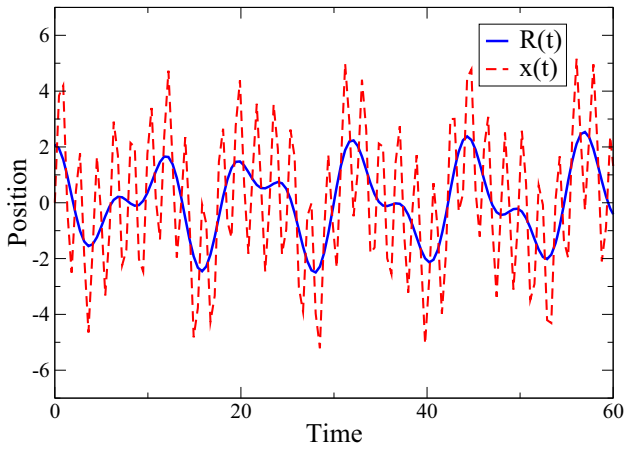

Fig. 1 The oscillatory motion of $x(t)$ around $R(t)$ for the model system in Eqs. (21)–(26) without any damping, i.e. for $\alpha = 0$ in Eq. (26). The initial value of $x(t)$ was set different from $R(t)$ to exaggerate the error. Without any dissipation there is no mechanism for the oscillations in $x(t)$ to decay and to get synchronized with $R(t)$ in a perfectly time-reversible integration

$$\begin{aligned}
\dot{\mathbf{R}}_I(t+\frac{\delta t}{2}) &= \dot{\mathbf{R}}_I(t) + \frac{\delta t}{2}\ddot{\mathbf{R}}_I(t),\\
\mathbf{R}_I(t+\delta t) &= \mathbf{R}_I(t) + \delta t\dot{\mathbf{R}}_I(t+\frac{\delta t}{2}),\\
n(t+\delta t) &= 2n(t) - n(t-\delta t) + \delta t^2\ddot{n}(t)\\
&\quad +\alpha\sum_{k=0}^{k_{\max}} c_k n(t-k\delta t),\\
\dot{\mathbf{R}}_I(t+\delta t) &= \dot{\mathbf{R}}_I(t+\frac{\delta t}{2}) + \frac{\delta t}{2}\ddot{\mathbf{R}}_I(t+\delta t), \quad (20)
\end{aligned}$$

where the coefficients, α and $\{c_k\}_{k=0}^{k_{\max}}$, as well as a dimensionless constant, $\kappa = \delta t^2\omega^2$, for various values of $k_{\max}$ are given in Ref. [84]. In the initial time step $n(t_0)$ and $n(t_0 - k\delta t)$ are all set to the fully converged regular Born–Oppenheimer ground state density, $\rho_0(\mathbf{r})$, at t_0.

The electronic dissipative force term, proportional to α in Eq. (20), breaks time-reversibility to a higher odd-order in the integration time step δt. The dissipative force term is constructed to be time reversible only up to some specific odd-order in δt, i.e. such that all lower odd-orders in δt are vanishing. In this way it is similar in spirit to the always stable predictor corrector scheme by Kolafa [81,107] and the Fock matrix dynamics schemes by Pulay [70,80]. However, instead of restoring an approximate time-reversal symmetry for a time-irreversible extrapolation, the scheme above breaks time-reversibility in an otherwise perfectly time-reversible Born–Oppenheimer dynamics [13]. The hybrid leapfrog velocity Verlet algorithm in Eq. (20) is in many ways just an ad hoc solution without a rigorous theoretical underpinning and can therefore be expected to be replaced by some more justifiable method. Nevertheless, it works surprisingly well.

3.6 Harmonic oscillator model

To illustrate the mechanics of the extended Lagrangian formulation and the modified hybrid leapfrog velocity Verlet integration scheme in Eq. (20) we can study a simple (unit-less) toy model, where we let an oscillatory nuclear motion,

$$R(t) = \sum_{k=1}^{4} A_k \cos(\Omega_k t), \quad (21)$$

$$A_1 = 1, \quad A_2 = \frac{23}{17}, \quad A_3 = -\frac{53}{73}, \quad A_4 = \frac{17}{37} \quad (22)$$

$$\Omega_1 = 1, \quad \Omega_2 = \frac{17}{31}, \quad \Omega_3 = \frac{127}{257}, \quad \Omega_4 = \frac{19}{31} \quad (23)$$

be accompanied by and auxiliary dynamical variable, $x(t)$, that follows the motion of $R(t)$ through a harmonic oscillator centered around $R(t)$. We define this dynamics for $x(t)$ with the Lagrangian,

$$\mathcal{L}(x,\dot{x}) = \frac{\mu}{2}\dot{x}^2(t) - \frac{\mu w^2}{2}\left(R(t) - x(t)\right)^2, \quad (24)$$

which gives us the equation of motion,

$$\ddot{x}(t) = \omega^2\left(R(t) - x(t)\right). \quad (25)$$

This model system is very similar to what we use in XL-BOMD, where the density, $n(t)$, which is evolving around the electronic ground state density determined by the atomic positions, is replaced by $x(t)$ oscillating around $R(t)$. The equation of motion for $x(t)$ in Eq. (25) can, therefore, also be integrated with the damped Verlet scheme in Eq. (20), where

$$\begin{aligned}
x(t+\delta t) &= 2x(t) - x(t-\delta t) + \delta t^2\omega^2\left(R(t) - x(t)\right)\\
&\quad +\alpha\sum_{k=0}^{K} c_k x(t-k\delta t). \quad (26)
\end{aligned}$$

We can use this harmonic oscillator model and the integration scheme above to understand the requirements for an adiabatic separation between $R(t)$ and $x(t)$. This separation can be fulfilled for a constant and system-independent value of the dimensionless variable $\kappa = \delta t^2\omega^2$ and the fact that we have to choose δt as some fraction of the fastest period, T, of the nuclear degrees of freedom, $R(t)$. In this way we can have a system-independent adiabatic separation between ω and the fastest nuclear frequency, $\Omega_1 = 1$, as long as the κ-value is sufficiently high. With a constant $\kappa = \delta t^2\omega^2 = 1.84$ and with ω chosen to be separated from Ω_1 by a factor of 3, i.e. with $\omega = 3\Omega_1$ such that $\delta t = \sqrt{\kappa/\omega^2} \approx 0.452$, then the shortest period, $T = 2\pi/\Omega_1$ of the nuclear motion, $R(t)$, is integrated in about 14 integration time steps, since $T/dt \approx 13.9$. This is a fairly typical choice for a Verlet integration.

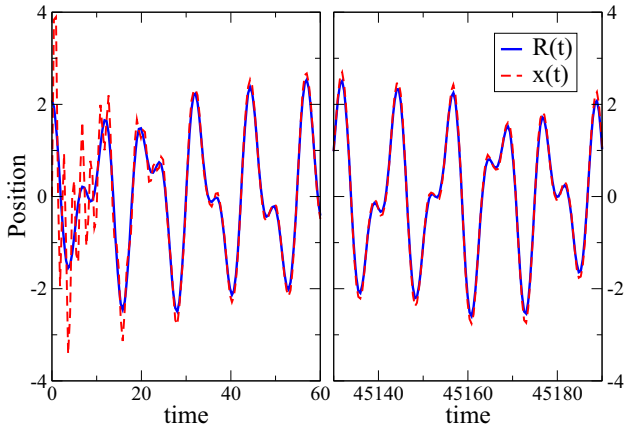

Fig. 2 The oscillatory motion of $x(t)$ around $R(t)$ for the model system in Eqs. (21)–(26) with and initial damping using $\alpha = 0.0055$ in Eq. (26) in the first 100 MD time steps ($t \leq 45$). The initial value of $x(t)$ was set different from $R(t)$ to exaggerate the error. The finite damping term reduces the oscillations in $x(t)$ that get synchronized with $R(t)$ through the dissipation. The damping term is turned off after the first 100 MD time steps ($t \approx 45$), but the synchronization is still kept after about 100,000 time steps, as shown in the right panel

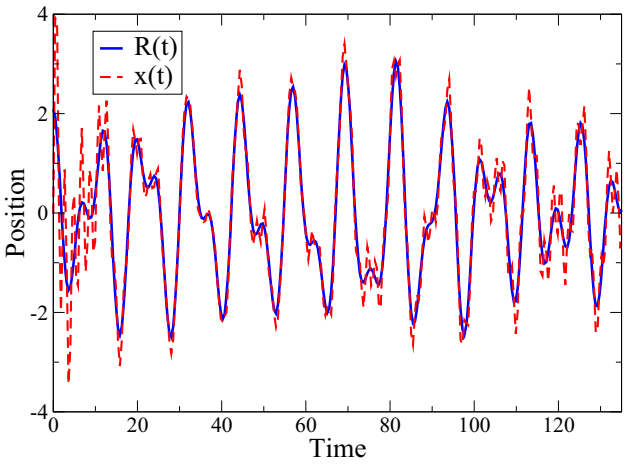

Fig. 3 The oscillatory motion of $x(t)$ around $R(t)$ for the model system in Eqs. (21)–(26) with an initial damping using $\alpha = 0.0055$ in Eq. (26) in the first 100 MD time steps ($t \leq 45$). The initial value of $x(t)$ was set different from $R(t)$ to exaggerate the error and an additional numerical noise term, $\xi(t) \in [-0.1, 0.1]$, is added to $x(t)$ in each time step. The damping term is used only during the first 100 MD time steps, after which it is turned off ($t \approx 45$). We then see a slow but steady increase in the deviation between $x(t)$ and $R(t)$ because of the noise accumulation

If we instead chose a shorter integration time step, the adiabatic separation between ω and Ω_1 increases with the value of κ kept fixed. In this way we always have an automatic separation in the frequencies between the harmonic oscillator and the fastest nuclear motion as long as we take normal integration times steps. The frequency separation would increase if we increased the value of κ. However, for the Verlet integration scheme there is an upper stability limit with $\kappa \leq 2$ [84].

To illustrate the properties of the modified Verlet integration scheme we can look at some simulation examples for the harmonic oscillator model. For the parameters we choose the optimized values in Ref. [84], where $\kappa = 1.84$, $c_0 = -14$, $c_1 = 36$, $c_2 = -27$, $c_3 = -2$, $c_4 = 12$, $c_5 = -6$, $c_6 = 1$ and $\alpha = 0.0055$. We use the same integration time step as above, $\delta t = \sqrt{\kappa/\omega^2} \approx 0.452$, which gives us the frequency separation where $\omega = 3\Omega_1$. In Fig. 1 we first show what happens without the dissipative force term, i.e. when $\alpha = 0$. Starting with an initial guess for $x(t) \neq R(t)$ there are significant oscillations in $x(t)$ around $R(t)$. The integration is perfectly time reversible and there is no mechanism for these oscillations to decay. This may indicate a poor behavior of XL-BOMD [106], but this is not the case if a more careful integration scheme is used. The left panel of Fig. 2 shows what happens when the damping term is turned on with $\alpha = 0.0055$. The amplitude of the oscillatory difference between $x(t)$ and $R(t)$ decays and the trajectory of $x(t)$ becomes synchronized with $R(t)$. After 100 MD time steps ($t \approx 45$) the damping is turned off. The right panel of Fig. 2 shows how the synchronization is still kept after about 100,000 MD time steps. In quantum based molecular dynamics simulations there is often a significant amount of numerical noise and without a continuous damping the synchronization between the electronic and the nuclear motion will eventually be lost. This effect is illustrated in Fig. 3, where we include an additional random (uniformly distributed) numerical noise term, $\xi(t) \in [-0.1, 0.1]$, that is added to $x(t)$ in each time step. When the initial damping is turned off after the first 100 MD time steps the error starts to accumulate. Eventually the synchronization is

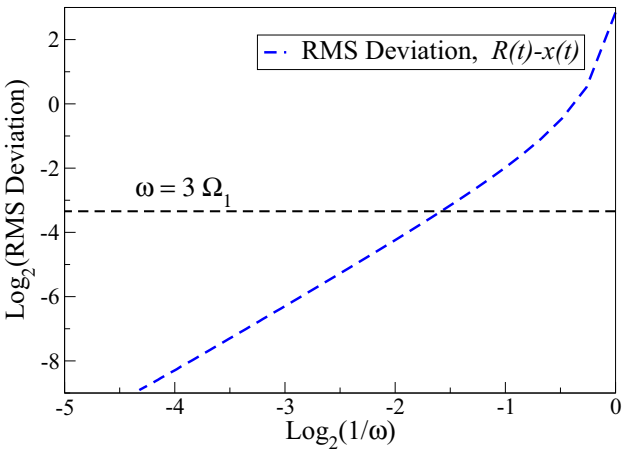

Fig. 4 The root mean square (RMS) deviation between the oscillatory motion of $x(t)$ and $R(t)$ for the model system in Eqs. (21)–(26) as a function of the adiabatic separation between $\Omega_1 = 1$ and ω. The deviation between $x(t)$ and $R(t)$ scales approximately as $|R(t) - x(t)| \sim 1/\omega^2$ as long as $\omega > \Omega_1 = 1$. The black dashed horizontal line shows the error for $\omega = 3\Omega_1$

completely lost. Only by keeping some dissipation is it possible to avoid the noise accumulation.

The three Figs. 1, 2 and 3 illustrates some of the most important properties of the extended Lagrangian schemes and the integration of the equations of motion, where $x(t)$ is following the motion of $R(t)$ through the evolution of a harmonic oscillator centered around $R(t)$. Another important property of this toy model is the scaling of $|R(t) - x(t)| \propto (\Omega_1/\omega)^2$ in the adiabatic limit. This is easy to show through a direct simulation of the harmonic oscillator model system, which is illustrated in Fig. 4. The same scaling is found in XL-BOMD, where the residual function behaves as $|\varrho[n] - n| \propto 1/\omega^2$, which leads to an error in the shadow Born–Oppenheimer potential that scales as $\mathcal{O}(\delta t^4)$ [26].

Unfortunately, the damping term in the modified Verlet integration breaks time-reversibility and for long enough simulations a noticeable systematic drift in the total energy (not shown) eventually appears. For QMD simulations this time limit it typically not reached in practice. However, in applications of XL-BOMD to polarizable force fields or charge equilibration models this can become a serious limitation. The UC Berkeley group headed by Teresa Head-Gordon has made significant progress trying to overcome some of these limitations with physics based approaches, where, for example, the electronic degrees of freedom is thermostated using Nose–Hoover or a Langevin dynamics [24,43–45,108].

3.7 Preconditioned Newton–Krylov method

The equations of motion for the extended electronic degrees of freedom in Eq. (18) include a kernel, $K(\mathbf{r},\mathbf{r'})$, that acts on the residual function, $(\varrho_0[n](\mathbf{r'}) - n(\mathbf{r'}))$. In a discrete matrix-vector generalization the corresponding equation of motion is given by

$$\ddot{\mathbf{n}} = -\omega^2 \mathbf{K}\,(\boldsymbol{\varrho}_0[\mathbf{n}] - \mathbf{n}), \tag{27}$$

where $\mathbf{K} \in R^{N\times N}$ and $\boldsymbol{\varrho}_0[\mathbf{n}] : R^N \rightarrow R^N$. If we use the vector function, $\mathbf{f}(\mathbf{n}) = (\boldsymbol{\varrho}_0[\mathbf{n}] - \mathbf{n}) : R^N \rightarrow R^N$, for the residual function, the kernel, $\mathbf{K}$, is given as the matrix inverse of the Jacobian, $\mathbf{J}$, of $\mathbf{f}(\mathbf{n})$, i.e.

$$\begin{aligned} J_{ij} &= \frac{\partial f_i(\mathbf{n})}{\partial n_j}, \\ \mathbf{K} &= \mathbf{J}^{-1}. \end{aligned} \tag{28}$$

The Jacobian matrix elements can be calculated with quantum perturbation theory [28,109–111], where each charge perturbation, n_i, gives rise to a Coulomb potential of the linearized electronic density functional, $\mathcal{E}_{\mathrm{DFT}}$ in Eq. (9), which generates a response in the optimized density, $\boldsymbol{\varrho}_0[n]$, as in Eq. (10). In this way the Jacobian matrix can be build column by column and the kernel $\mathbf{K}$ is then given by the matrix inversion. The full calculation of the kernel is computationally expensive, especially if it would be performed in each time step, and instead various approximations are used. The easiest technique is to approximate the kernel with a scaled delta-function, where

$$K(\mathbf{r},\mathbf{r'}) = -c\delta(\mathbf{r}\text{-}\mathbf{r'}), \quad c \in [0,1]. \tag{29}$$

This simple approximation works well for a broad range of problems. However, more advanced approaches are required for systems that exhibit intrinsic instabilities with charge sloshing or reactions with opening and closing of the electronic gap between the highest occupied molecular orbital (HOMO) and the lowest unoccupied molecular orbital (LUMO).

The regular definition of the Jacobian in Eq. (28) is based on partial derivatives with respect to the different components of $\mathbf{n} = \{n_j\}$. This definition can be generalized [28] using a set of arbitrary directional derivatives,

$$\mathbf{f}_{\mathbf{v}_i}(\mathbf{n}) \equiv \left.\frac{\partial \mathbf{f}(\mathbf{n} + \lambda \mathbf{v}_i)}{\partial \lambda}\right|_{\lambda=0}. \tag{30}$$

We can express the Jacobian in terms of such generalized directional derivatives as

$$\mathbf{J} = \sum_{i,j=1}^{N} \mathbf{f}_{\mathbf{v}_i} L_{ij} \mathbf{v}_j^T, \tag{31}$$

where $\mathbf{L} = \mathbf{O}_v^{-1}$ is the inverse of the overlap matrix $\mathbf{O}_v$ with matrix elements $O_{vij} = \mathbf{v}_i^T \mathbf{v}_j$. The $\mathbf{n}$-dependence in $\mathbf{f}_{\mathbf{v}_i} \equiv \mathbf{f}_{\mathbf{v}_i}(\mathbf{n})$ has been dropped for simplicity. The generalized Jacobian in Eq. (31) can be used to define a rank-m approximation of the Jacobian, where

$$\mathbf{J}_m = \sum_{i,j=1}^{m} \mathbf{f}_{\mathbf{v}_i} L_{ij} \mathbf{v}_j^T, \quad m \leq N, \tag{32}$$

from which we can construct a low-rank approximation of the kernel, $\mathbf{K}_m$, through a Moore–Penrose pseudoinverse of $\mathbf{J}_m$, where

$$\mathbf{K}_m = \sum_{i,j=1}^{m} \mathbf{v}_i M_{ij} \mathbf{f}_{\mathbf{v}_j}^T, \quad m \leq N. \tag{33}$$

The matrix $\mathbf{M} = \mathbf{O}_f^{-1}$ is here the inverse of the overlap matrix, $\mathbf{O}_f$, with elements $O_{f\,ij} = \mathbf{f}_{\mathbf{v}_i}^T \mathbf{f}_{\mathbf{v}_j}$. A low-rank kernel approximation from the inverse of the generalized Jacobian can then be used in the integration of the equations of motion, Eq. (27), where only a few directional derivatives are used instead of a complete set of response calculations with respect to $\{n_i\}$ [28]. Each directional response calculation can be performed using quantum perturbation theory. For systems with fractional occupation numbers special care is needed to capture the response also in the occupation and the chemical potential [28,110,111]. To keep the cost low in the low-rank kernel approximation in Eq. (33) we need

to keep the number of directional derivatives as low as possible. This can be achieved using preconditioning.

If we have access to some approximation to the inverse Jacobian, $\mathbf{K}_0 \approx \mathbf{J}^{-1}$, we may rewrite the equations of motion, Eq. (27), in an equivalent form,

$$\ddot{\mathbf{n}} = -\omega^2 \left(\mathbf{K}_0\mathbf{J}\right)^{-1} \mathbf{K}_0 \left(\boldsymbol{\varrho}_0[\mathbf{n}] - \mathbf{n}\right). \tag{34}$$

Instead of finding some low-rank approximation of $\mathbf{K} = \mathbf{J}^{-1}$ acting on the residual vector $\mathbf{f}[\mathbf{n}] = (\boldsymbol{\varrho}_0[\mathbf{n}] - \mathbf{n})$, we can then calculate a low-rank approximation of $(\mathbf{K}_0\mathbf{J})^{-1}$ acting on the preconditioned residual $\mathbf{K}_0\mathbf{f}[\mathbf{n}]$. The corresponding preconditioned Jacobian is then given by

$$\mathbf{K}_0\mathbf{J} \approx \sum_{i,j=1}^{n} \left(\mathbf{K}_0\mathbf{f}_{\mathbf{v}_i}\right) L_{i,j}\mathbf{v}_j^T \equiv \sum_{i,j=1}^{n} \widetilde{\mathbf{f}}_{\mathbf{v}_i} L_{i,j}\mathbf{v}_j^T, \tag{35}$$

with the pseudoinverse

$$\widetilde{\mathbf{K}} = \left(\mathbf{K}_0\mathbf{J}\right)^{-1} \approx \sum_{i,j=1}^{m} \mathbf{v}_i \widetilde{M}_{i,j} \widetilde{\mathbf{f}}_{\mathbf{v}_j}^T, \quad m \leq N, \tag{36}$$

where $\widetilde{\mathbf{M}} = \mathbf{O}_{\widetilde{f}}^{-1}$. This preconditioned low-rank approximation of $\mathbf{K}$ can then be used in the equations of motion,

$$\ddot{\mathbf{n}} \approx -\omega^2 \left(\sum_{i,j=1}^{m} \mathbf{v}_i \widetilde{M}_{i,j} \widetilde{\mathbf{f}}_{\mathbf{v}_j}^T \right) \mathbf{K}_0 \left(\mathbf{q}[\mathbf{n}]\text{-}\mathbf{n}\right), \quad m \leq N, \tag{37}$$

which is exact in the full-rank limit when $m = N$. The problem is now how we can choose the directional derivatives, $\{\mathbf{v}_i\}$ and $\{\widetilde{\mathbf{f}}_{\mathbf{v}_j}\}$, in some optimal way such that the error is small while the rank still can be kept low. Probably the only reasonable and best possible way is from an orthogonalized Krylov subspace, $\mathcal{K}^{\perp}$, where

$$\{\mathbf{v}_i\} \in \mathcal{K}^{\perp} = \text{span}^{\perp} \left\{\mathbf{K}_0\mathbf{f}(\mathbf{n}), (\mathbf{K}_0\mathbf{J})\mathbf{K}_0\mathbf{f}(\mathbf{n}), (\mathbf{K}_0\mathbf{J})^2\mathbf{K}_0\mathbf{f}(\mathbf{n}), \ldots\right\}. \tag{38}$$

Here $\text{span}^{\perp}$ indicates the orthogonalized span, where for each new vector in the subspace only the orthogonal complement to the previous vectors is kept. The vectors, $\{\mathbf{v}_i\}$ and $\{\widetilde{\mathbf{f}}_{\mathbf{v}_j}\}$, can then be generated using the relations:

$$\mathbf{J}\mathbf{u} = \left.\frac{\partial \mathbf{f}(\mathbf{n} + \lambda\mathbf{u})}{\partial\lambda}\right|_{\lambda=0} \equiv \mathbf{f}_{\mathbf{u}}, \qquad \widetilde{\mathbf{f}}_{\mathbf{u}} = \mathbf{K}_0\mathbf{f}_{\mathbf{u}}. \tag{39}$$

The low-rank preconditioned Krylov subspace approximation of the kernel provides an efficient approach to integrate the electronic equations of motion in Eq. (18) or as in Eq. (27). In combination with fractional occupation numbers it allows stable QMD simulations of systems that normally would be a major challenge also for regular direct BOMD simulations [28,29].

The ability to generate low-rank approximations of the pseudoinverse of a generalized Jacobian with directional derivatives chosen from a Krylov subspace is a highly powerful methodology. Applied in combination with Newton's method for the solution of non-linear equations it can be used to derive Broyden's class of algorithms, including Anderson and Pulay mixing, and for linear systems of equations it automatically generates minimum residual methods [112–117]. In this way, the low-rank preconditioned Krylov subspace approximation of the generalized inverse Jacobian presented above provides a transparent and unifying theory for a number of frequently used methods. A more detailed discussion in given in Ref. [28].

4 XL-BOMD for thermal Hartree–Fock theory: a density matrix formulation

XL-BOMD defined by the Lagrangian in Eq. (13) was presented with a shadow Born–Oppenheimer potential derived from the universal Hohenberg–Kohn density functional, $F[n]$, for the electronic energy and with the electronic density, $n(\mathbf{r})$, as a dynamical field variable. Different forms of XL-BOMD can then be constructed by replacing the universal functional with, for example, the Kohn–Sham formulation [87,88,118] and the electron density can be substituted with, for example, the molecular orbitals [15] or the density matrix [20,21,34,41]. We may alternatively apply XL-BOMD together with thermal Hartree–Fock theory with the electronic degrees of freedom represented by a density matrix, which will be presented in this section. Hartree–Fock theory is derived from an ansatz of the many-body electron wavefunction that is formed by a single Slater determinant. This leads to an electron-electron interaction that consists of a mean-field Hartree term corresponding to the electrostatic Coulomb energy for the electron density plus an exchange term governed by the anti-symmetry of the determinant wavefunction. The many-body wavefunction formulation can then be cast into a mean-field single-electron picture where the electronic energy is given from a constrained minimization of a density-matrix energy functional [119–121]. Hartree–Fock theory provides a natural example of how a density matrix can be used to represent the electronic degrees of freedom instead of the density or the wavefunctions. This makes the Hartree–Fock formalism generally applicable to a broad range of electronic structure methods.

To present XL-BOMD based on thermal Hartree–Fock theory using the density matrix formalism we first describe the regular Born–Oppenheimer formulation, where we assume an instantaneous thermal equilibra-

tion of the electrons using a spin-restricted model. We then present how XL-BOMD can be constructed. Complementary descriptions are given in Refs. [29,32].

4.1 Born–Oppenheimer MD for thermal Hartree–Fock theory

The electronic free energy in spin-restricted, thermal Hartree–Fock theory [87,122], assuming an instantaneous thermal equilibration of the electrons for each new atomic position, can be described in terms of a density matrix function [119],

$$E_{\rm HF}(\mathbf{R},\mathbf{D}) = 2{\rm Tr}[\mathbf{hD}] + {\rm Tr}[\mathbf{DG}(\mathbf{D})] \\ -2T_e\mathcal{S}(\mathbf{D}^\perp) - \mu_e\left(2{\rm Tr}[\mathbf{D}^\perp] - N_{\rm occ}\right). \tag{40}$$

We here assume a finite basis-set representation of the operators, $X_{ij} = \langle\phi_i|\hat{X}|\phi_j\rangle$ using some underlying atom-centered finite basis-set, $\{\phi_i(\mathbf{r})\}_{i=1}^N$, with overlap matrix $S_{ij} = \langle\phi_i|\phi_j\rangle$. $\mathbf{D} \in R^{N\times N}$ is the single-particle density matrix, T_e is the electronic temperature, μ_e is the chemical potential, $N_{\rm occ}$ is the number of occupied orbitals (two electrons in each), $\mathbf{h}$ is the charge independent one-electron Hamiltonian, and $\mathbf{G}(\mathbf{D}) = 2\mathbf{J}(\mathbf{D}) - \mathbf{K}(\mathbf{D})$ is the combined Coulomb and exchange matrix [29,119]. The relation between the atomic-orbital representation of the density matrix, $\mathbf{D}$, and its orthogonal representation, $\mathbf{D}^\perp$, is given by $\mathbf{D} = \mathbf{Z}\mathbf{D}^\perp\mathbf{Z}^T$, where the inverse overlap factorization matrix, $\mathbf{Z}$, is determined by the requirement that $\mathbf{Z}^T\mathbf{S}\mathbf{Z} = \mathbf{I}$. For simplicity, we have chosen the entropy term $\mathcal{S}(\mathbf{D}^\perp)$, in Eq. (40), as a function of the density matrix in its orthogonal representations, where

$$\mathcal{S}(\mathbf{D}^\perp) = -k_B{\rm Tr}\left[\mathbf{D}^\perp\ln\mathbf{D}^\perp + (\mathbf{I}-\mathbf{D}^\perp)\ln(\mathbf{I}-\mathbf{D}^\perp)\right]. \tag{41}$$

The Born–Oppenheimer potential energy surface is given by the stationary minima,

$$U_{\rm BO}^{\rm HF}(\mathbf{R}) = \min_{\mathbf{D}}\{E_{\rm HF}(\mathbf{R},\mathbf{D})\} + V_{nn}(\mathbf{R}), \tag{42}$$

including the nuclear–nuclear repulsion term, $V_{nn}(\mathbf{R})$. The ground-state density matrix that minimizes the free energy in Eq. (42) is given in an implicit form as

$$\mathbf{D}^\perp = \left[e^{\beta(\mathbf{F}^\perp(\mathbf{D})-\mu_e\mathbf{I})} + \mathbf{I}\right]^{-1}. \tag{43}$$

Here $\beta = (k_BT_e)^{-1}$ is the inverse electronic temperature and the density-matrix dependent Fockian,

$$\mathbf{F}(\mathbf{D}) = \mathbf{h} + \mathbf{G}(\mathbf{D}), \tag{44}$$

is used in its orthogonalized representation, where $\mathbf{F}^\perp(\mathbf{D}) = \mathbf{Z}^T\mathbf{F}(\mathbf{D})\mathbf{Z}$. The ground-state density matrix in Eq. (43) is thus given only implicitly and it can only be constructed by some iterative self-consistent field optimization procedure, which is costly and in practice never exact. It is easy to show that the free energy in Eq. (40) is stationary for the self-consistent solution in Eq. (43) from the vanishing matrix derivative of the free energy term,

$$\frac{\partial E_{\rm HF}(\mathbf{R},\mathbf{D})}{\partial\mathbf{D}^\perp} \\ = 2\mathbf{h}^\perp + 2\mathbf{G}^\perp(\mathbf{D}) - 2(\mathbf{F}^\perp(\mathbf{D}) - \mu_e\mathbf{I}) - 2\mu_e\mathbf{I} = 0, \tag{45}$$

where we used the relation that

$$\begin{aligned}\frac{\partial\mathcal{S}(\mathbf{D}^\perp)}{\partial\mathbf{D}^\perp} &= -k_B\left(\ln\mathbf{D}^\perp + \mathbf{I} - \ln(\mathbf{I}-\mathbf{D}^\perp) - \mathbf{I}\right)\\ &= -k_B\ln\left(\frac{\mathbf{D}^\perp}{\mathbf{I}-\mathbf{D}^\perp}\right)\\ &= -k_B\ln\left(e^{\beta(\mathbf{F}^\perp(\mathbf{D})-\mu_e\mathbf{I})} + \mathbf{I}\right)\\ &= \beta k_B(\mathbf{F}^\perp(\mathbf{D}) - \mu_e\mathbf{I}).\end{aligned} \tag{46}$$

A thermal Hartree–Fock based Born–Oppenheimer MD can then be defined with the Lagrangian

$$\mathcal{L}(\mathbf{R},\dot{\mathbf{R}}) = \frac{1}{2}\sum_I M_I|\dot{\mathbf{R}}_I|^2 - U_{\rm BO}^{\rm HF}(\mathbf{R}), \tag{47}$$

with the equations of motion

$$M_I\ddot{\mathbf{R}}_I = -\nabla_R U_{\rm BO}^{\rm HF}(\mathbf{R}). \tag{48}$$

The potential gradient evaluation that is needed for the forces,

$$-\nabla_R U_{\rm BO}^{\rm HF}(\mathbf{R}) = -\nabla_R E_{\rm HF}(\mathbf{R},\mathbf{D}) - \nabla_R V_{nn}(\mathbf{R}), \tag{49}$$

requires the gradient of the free energy term,

$$\nabla_R E_{\rm HF}(\mathbf{R},\mathbf{D}) = 2{\rm Tr}[\mathbf{h}_R\mathbf{D}] + 2{\rm Tr}[\mathbf{h}\mathbf{D}_R] + 2{\rm Tr}[\mathbf{D}_R\mathbf{G}(\mathbf{D})] \\ +{\rm Tr}[\mathbf{D}\mathbf{G}_R(\mathbf{D})] - 2T_e\nabla_R\mathcal{S}(\mathbf{D}^\perp) - 2\mu_e{\rm Tr}[\mathbf{D}_R^\perp], \tag{50}$$

where we use the notation, $\nabla_R\mathbf{X} = \mathbf{X}_R$. Together with the entropy gradient,

$$\begin{aligned}\nabla_R\mathcal{S}(\mathbf{D}^\perp) &= -k_B{\rm Tr}\left[\mathbf{D}_R^\perp\ln\mathbf{D}^\perp + \mathbf{R}_R^\perp \right.\\ &\qquad \left. -\mathbf{R}_R^\perp\ln(\mathbf{I}-\mathbf{D}^\perp) - \mathbf{D}_R^\perp\right]\\ &= -k_B{\rm Tr}\left[\mathbf{D}^\perp\ln\left(\frac{\mathbf{D}^\perp}{\mathbf{I}-\mathbf{D}^\perp}\right)\right]\\ &= -k_B{\rm Tr}\left[\mathbf{D}_R^\perp\ln\left(e^{\beta(\mathbf{F}^\perp-\mu_e\mathbf{I})}\right)\right]\\ &= \beta k_B{\rm Tr}\left[\mathbf{D}_R^\perp\mathbf{F}^\perp\right] - \beta k_B{\rm Tr}\left[\mu_e\mathbf{D}_R^\perp\right],\end{aligned} \tag{51}$$

and the definition of the Fockian, $\mathbf{F} = \mathbf{h} + \mathbf{G}(\mathbf{D})$, we find that

$$\nabla_R E_{\rm HF}(\mathbf{R},\mathbf{D}) = 2{\rm Tr}[\mathbf{h}_R\mathbf{D}] + {\rm Tr}[\mathbf{D}\mathbf{G}_R(\mathbf{D})] + 2{\rm Tr}[\mathbf{F}\mathbf{D}_R] - 2{\rm Tr}[\mathbf{F}^{\perp}\mathbf{D}_R^{\perp}]. \quad (52)$$

The derivative, $\mathbf{D}_R$, in the third term on the right-hand side of Eq. (52) can then be determined from its orthogonal representation, where

$$\begin{aligned}\mathbf{D}_R &= \nabla_R\left(\mathbf{Z}\mathbf{D}^{\perp}\mathbf{Z}^T\right)\\ &= \mathbf{Z}_R\mathbf{D}^{\perp}\mathbf{Z}^T + \mathbf{Z}\mathbf{D}_R^{\perp}\mathbf{Z}^T + \mathbf{Z}\mathbf{D}^{\perp}\mathbf{Z}_R^T\\ &= -\frac{1}{2}\mathbf{S}^{-1}\mathbf{S}_R\mathbf{Z}\mathbf{D}^{\perp}\mathbf{Z}^T + \mathbf{Z}\mathbf{D}_R^{\perp}\mathbf{Z}^T\\ &\quad -\frac{1}{2}\mathbf{Z}\mathbf{D}^{\perp}(\mathbf{S}^{-1}\mathbf{S}_R\mathbf{Z})^T. \end{aligned} \quad (53)$$

Here we used the non-trivial relation that $\mathbf{Z}_R = -(1/2)\mathbf{S}^{-1}\mathbf{S}_R\mathbf{Z}$ (see Refs. [123,124]). This means that in Eq. (52) the third term on the right-hand side can be rewritten as

$$\begin{aligned}2{\rm Tr}[\mathbf{F}\mathbf{D}_R] &= 2{\rm Tr}[\mathbf{F}\mathbf{Z}\mathbf{D}_R^{\perp}\mathbf{Z}^T] - {\rm Tr}[\mathbf{F}\mathbf{S}^{-1}\mathbf{S}_R\mathbf{D}]\\ &\quad -{\rm Tr}[\mathbf{F}\mathbf{D}\mathbf{S}_R\mathbf{S}^{-1}]\\ &= 2{\rm Tr}[\mathbf{F}^{\perp}\mathbf{D}_R^{\perp}] - 2{\rm Tr}[\mathbf{S}^{-1}\mathbf{F}\mathbf{D}\mathbf{S}_R], \end{aligned} \quad (54)$$

where we used the commutation relation, $\mathbf{SDF - FDS = 0}$, or that $\mathbf{DFS}^{-1} - \mathbf{S}^{-1}\mathbf{FD} = \mathbf{0}$. Inserted into Eq. (52), we then get the final expression for the gradient of the free energy for thermal Hartree–Fock theory,

$$-\nabla_R E_{\rm HF}(\mathbf{R},\mathbf{D}) = -2{\rm Tr}[\mathbf{h}_R\mathbf{D}] - {\rm Tr}[\mathbf{D}\mathbf{G}_R(\mathbf{D})] + 2{\rm Tr}[\mathbf{S}^{-1}\mathbf{F}\mathbf{D}\mathbf{S}_R], \quad (55)$$

where the last term can be seen a generalized Pulay force term [124–126]. This force term can then be used to integrate the equations of motion in Eq. (48) for the Born–Oppenheimer molecular dynamics scheme based on thermal Hartree–Fock theory. The main cost in each time step is the self-consistent calculation of the ground state density matrix in Eq. (43). The main part of this overhead can be avoided by applying the framework of XL-BOMD.

4.2 XL-BOMD for thermal Hartree–Fock

To construct XL-BOMD based on the thermal Hartree–Fock theory presented above, we first need to find an approximate shadow free energy function, $\mathcal{E}_{\rm HF} \approx E_{\rm HF}$ [29]. We can achieve this with a linearization of the free energy expression, $E_{\rm HF}(\mathbf{R},\mathbf{D})$ in Eq. (40), around some approximate solution, $\mathbf{P}$, to the exact self-consistent density matrix, which gives us the shadow energy function

$$\mathcal{E}_{\rm HF}(\mathbf{R},\mathbf{D},\mathbf{P}) = 2{\rm Tr}[\mathbf{h}\mathbf{D}] + {\rm Tr}[(\mathbf{2D-P})\mathbf{G}(\mathbf{P})] - 2T_e\mathcal{S}(\mathbf{D}^{\perp}) - \mu_e\left(2{\rm Tr}[\mathbf{D}^{\perp}] - N_{\rm occ}\right). \quad (56)$$

With the $\mathbf{P}$-dependent density matrix, $\mathbf{D}$, given by the direct explicit construction,

$$\begin{aligned}\mathbf{F}^{\perp}(\mathbf{P}) &= \mathbf{Z}^T\left(\mathbf{h} + \mathbf{G}(\mathbf{P})\right)\mathbf{Z},\\ \mathbf{D}^{\perp}[\mathbf{P}] &= \left[e^{\beta(\mathbf{F}^{\perp}(\mathbf{P})-\mu_e\mathbf{I})} + \mathbf{I}\right]^{-1},\\ \mathbf{D}[\mathbf{P}] &= \mathbf{Z}\mathbf{D}^{\perp}[\mathbf{P}]\mathbf{Z}^T, \end{aligned} \quad (57)$$

it is easy to show that

$$\left.\frac{\partial\mathcal{E}_{\rm HF}(\mathbf{R},\mathbf{D},\mathbf{P})}{\partial\mathbf{D}^{\perp}}\right|_{\mathbf{D}^{\perp}[\mathbf{P}]} = 2\mathbf{h}^{\perp} + 2\mathbf{G}^{\perp}(\mathbf{P}) - 2(\mathbf{F}^{\perp}(\mathbf{P}) - \mu_e\mathbf{I}) - 2\mu_e\mathbf{I} = \mathbf{0}. \quad (58)$$

A shadow Born–Oppenheimer potential energy,

$$\mathcal{U}_{\rm BO}^{\rm HF}(\mathbf{R},\mathbf{P}) = \min_{\mathbf{D}}\left\{\mathcal{E}_{\rm HF}(\mathbf{R},\mathbf{D},\mathbf{P})\right\} + V_{nn}(\mathbf{R})\}, \quad (59)$$

can therefore be constructed without any approximate iterative optimization process. Instead, only a single direct density-matrix calculation, $\mathbf{P} \to \mathbf{D}[\mathbf{P}]$, in Eq. (57) is needed. As long as $\mathbf{P} \approx \mathbf{D}[\mathbf{P}]$ we can, therefore, calculate a good approximation to the exact self-consistent Born–Oppenheimer potential in a single step using the explicit definition of the density matrix in Eq. (57). We can then define an XL-BOMD with the Lagrangian,

$$\begin{aligned}\mathcal{L}_{\rm XBO}(\mathbf{R},\dot{\mathbf{R}},\mathbf{X},\dot{\mathbf{X}}) &= \frac{1}{2}\sum_I M_I|\mathbf{R}_I|^2 - \mathcal{U}_{\rm BO}^{\rm HF}(\mathbf{R},\mathbf{X}\mathbf{S}^{-1})\\ &\quad +\frac{1}{2}\mu{\rm Tr}[\dot{\mathbf{X}}^2] - \frac{1}{2}\mu\omega^2{\rm Tr}\left[(\mathbf{D}[\mathbf{X}\mathbf{S}^{-1}]\mathbf{S} - \mathbf{X})\right.\\ &\quad \left.\mathcal{T}((\mathbf{D}[\mathbf{X}\mathbf{S}^{-1}]\mathbf{S} - \mathbf{X})\right]. \end{aligned} \quad (60)$$

We have here chosen a dynamical variable $\mathbf{X} = \mathbf{PS}$ and its time derivative $\dot{\mathbf{X}}$. This provides a tensorially more accurate propagation [20]. In each time step we therefore transform $\mathbf{X}$ to the density matrix $\mathbf{P} = \mathbf{X}\mathbf{S}^{-1}$ prior to the energy and force evaluations. The metric tensor $\mathcal{T} = \mathcal{K}^T\mathcal{K} \in R^{N^2\times N^2}$ is a super matrix that transforms a matrix into a matrix, which is defined in the same way as previously from the inverse of the Jacobian of the residual matrix function, $\mathbf{f}(\mathbf{X}) = (\mathbf{D}[\mathbf{X}\mathbf{S}^{-1}]\mathbf{S} - \mathbf{X})$ [29]. The equations of motion can then be derived from the Euler–Lagrange equations in the adiabatic limit as $\omega \to \infty$ and $\mu \to 0$ such that $\mu\omega =$ constant. In this adiabatic limit we get the equations of motion,

$$\begin{aligned}M_I\ddot{\mathbf{R}}_I &= -\nabla_R\mathcal{U}_{\rm BO}^{\rm HF}(\mathbf{R},\mathbf{X}\mathbf{S}^{-1}),\\ \ddot{\mathbf{X}} &= -\omega^2\mathcal{K}\left(\mathbf{D}[\mathbf{X}\mathbf{S}^{-1}]\mathbf{S} - \mathbf{X}\right), \end{aligned} \quad (61)$$

where the gradient of the electronic free energy, $\nabla_R \mathcal{E}_{\rm HF}(\mathbf{R},\mathbf{D},\mathbf{P})$, [calculated for the stationary solution of $\mathbf{D} = \mathbf{D}[\mathbf{P}]$ in Eq. (57)] is given by a modified force expression similar to Eq. (55),

$$\begin{aligned}\nabla_R \mathcal{E}_{\rm HF}(\mathbf{R},\mathbf{D},\mathbf{P})|_{\mathbf{D}[\mathbf{P}]} \\ = 2{\rm Tr}[\mathbf{h}_R\mathbf{D}] + {\rm Tr}[(2\mathbf{D}-\mathbf{P})\mathbf{G}_R(\mathbf{X}\mathbf{S}^{-1})] \\ -2{\rm Tr}[\mathbf{S}^{-1}\mathbf{F}\mathbf{D}\mathbf{S}_R].\end{aligned} \tag{62}$$

An extra $\mathbf{S}^{-1}$-dependent gradient term,

$$2{\rm Tr}[\mathbf{X}\mathbf{S}_R^{-1}\mathbf{G}(\mathbf{D}-\mathbf{X}\mathbf{S}^{-1})], \tag{63}$$

also appears because of the switch of variables from $\mathbf{X}$ to $\mathbf{P} = \mathbf{X}\mathbf{S}^{-1}$, but this additional Pulay term vanish in the adiabatic limit as $|\mathbf{D}-\mathbf{X}\mathbf{S}^{-1}| \propto |\mathbf{D}\mathbf{S}-\mathbf{X}| \propto \omega^{-2}$. The simple gradient expression in Eq. (62) relies on the fact that $\mathbf{D}[\mathbf{P}]$ is a stationary solution to the shadow energy functional, Eq. (58), for $\mathbf{D} = \mathbf{D}[\mathbf{P}]$. The constant of motion in the adiabatic limit is

$$E^{\rm HF}_{\rm XBO} = \frac{1}{2}\sum_I M_I|\mathbf{R}_I|^2 + \mathcal{U}^{\rm HF}_{\rm BO}(\mathbf{R},\mathbf{X}\mathbf{S}^{-1}), \tag{64}$$

which closely follows the exact Born–Oppenheimer total energy as long as $\mathbf{X} \approx \mathbf{D}[\mathbf{X}\mathbf{S}^{-1}]\mathbf{S}$. A detailed algorithm description of this density-matrix based scheme, including low-rank approximations of the kernel $\mathcal{K}$ is given in Ref. [29]. The low-rank approximations of the kernel are important, because there is no practical way to calculate the full kernel, not even a single time, unless the system is very small. An efficient preconditioner for the density matrix formulation of XL-BOMD has not yet been developed.

4.3 Example

The simplest possible example illustrating a QMD simulation is probably a hydrogen molecule. Figure 5 shows an example of an XL-BOMD simulation based on thermal Hartree–Fock theory with an electronic temperature set to $T_e = 1500$ K, and where the hydrogen is released from a stretched configuration with the two atoms initially separated at about twice the equilibrium bond length, which significantly reduces the size of the estimated electronic gap. The gap is here estimated from the energy eigenvalue difference between the HOMO and LUMO states, i.e. as if the states had integer occupation numbers. The upper panel shows the interatomic distance, $R(t)$, as a function of time. The middle panel shows the fluctuations in the total energy and the lower panel shows the fluctuations in the electronic HOMO-LUMO gap corresponding to the integer occupation at zero electronic temperature. An adaptive low-rank approximation of the kernel was used as described in Ref. [29]. The integration time step was 0.25 fs and the total energy remains stable without any visible systematic drift, although the oscillations have sharp turning points around $R(t) \approx 1$ Bohr radius. As the molecule is stretched the electronic gap is sufficiently small such that the "LUMO" state becomes fractionally occupied. Its LUMO fractional occupation oscillates between the stretched and compressed turning points from about 0.2–0.02.

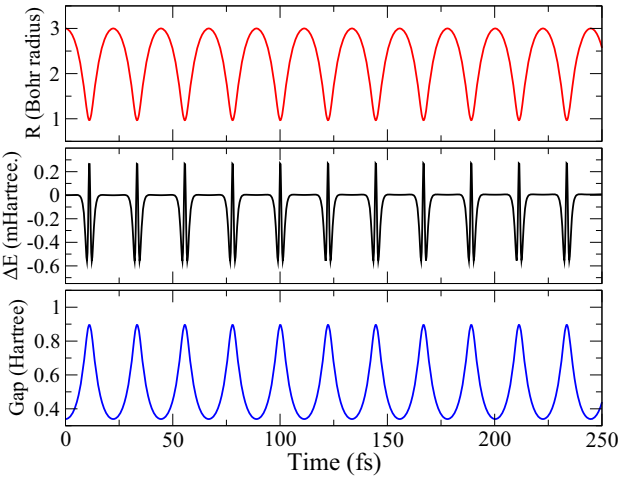

Fig. 5 QMD simulation of a hydrogen molecule using XL-BOMD based on thermal Hartree–Fock theory. A basis set of 8 uncontracted primitive Gaussian functions were used [127]. The electronic temperature was set to 1500 K and a time step of 0.25 fs was used, in combination with the modified Verlet integration scheme in Eq. (20)

5 XL-BOMD for SCC-DFTB

XL-BOMD can be adapted to a broad set of electronic structure models based on density-functional and Hartree–Fock theory, including semi-empirical methods [16,17,27,37,49]. Semi-empirical electronic structure calculations [128–134] are typically 2–3 orders of magnitude faster compared to ab initio calculations using density functional theory. The speedup is achieved using simplified approximate electronic structure models combined with flexible efficient parameterizations. By optimizing the parameterization based on experimental or high-level theoretical calculations using genetic algorithms [135,136], it is often possible to achieve an accuracy at a comparable level to high-level first principles methods. Modern machine learning tools [137–151] may further improve these techniques with the promise of an almost ideal combination of physically transparent and highly accurate models that allow computationally efficient simulations at only a fraction of the cost of current state-of-the-art ab initio methods.

A popular class of semi-empirical methods is density functional tight-binding (DFTB) theory [37,130,136,152–158]. DFTB theory can be seen as a framework for different levels of model approximations of density functional theory. A frequently used DFTB model is

given by a second-order expansion in the charge density fluctuations of the DFT energy functional, Eq. (1), around a reference density of overlapping neutral atomic charge distributions, where atomic net Mulliken charges are used to describe the long-range electrostatic interactions. The fluctuating charges are optimized self-consistently to account for interatomic charge transfer and the response to the electrostatic interactions. XL-BOMD works very well in combination with this level of second-order self-consistent charge density functional based tight-binding (SCC-DFTB) theory. Here we will give some background of this semi-empirical theory and how it can be combined with XL-BOMD.

5.1 SCC-DFTB theory

In SCC-DFTB theory a second-order expansion of the electronic density functional, $E_{\mathrm{DFT}}[\mathbf{R},\rho]$ in Eq. (1), is performed in the fluctuations, $\Delta\rho(\mathbf{r})$, around a reference electron density, $\rho_{\mathrm{ref}}(\mathbf{r})$, of overlapping neutral atomic densities. With the net charge density, $\rho(\mathbf{r}) = \rho_{\mathrm{ref}}(\mathbf{r}) + \Delta\rho(\mathbf{r})$, the second-order expansion of $E_{\mathrm{DFT}}[\mathbf{R},\rho]$, including the nuclear–nuclear repulsion, $v_{nn}(\mathbf{R})$, is given by

$$\begin{aligned} E_{\mathrm{DFT}}[\mathbf{R},\rho] + v_{nn}(\mathbf{R}) &= F[\rho] \\ &+ \int v_{\mathrm{ext}}(\mathbf{R},\mathbf{r})\rho(\mathbf{r})\mathrm{d}\mathbf{r} + v_{nn}(\mathbf{R}) \\ &= F[\rho_{\mathrm{ref}}] + \int v_{\mathrm{ext}}(\mathbf{R},\mathbf{r})\rho_{\mathrm{ref}}(\mathbf{r})\mathrm{d}\mathbf{r} + v_{nn}(\mathbf{R}) \\ &+ \int \left(\frac{\delta F[\rho]}{\delta\rho}\bigg|_{\rho_{\mathrm{ref}}} + v_{\mathrm{ext}}(\mathbf{R},\mathbf{r}) \right) \Delta\rho(\mathbf{r})\mathrm{d}\mathbf{r} \\ &+ \frac{1}{2}\iint \Delta\rho(\mathbf{r})\frac{\delta^2 F[\rho]}{\delta\rho^2}\bigg|_{\rho_{\mathrm{ref}}} \Delta\rho(\mathbf{r'})\mathrm{d}\mathbf{r}\mathrm{d}\mathbf{r'} + \mathcal{O}(\Delta\rho^3). \end{aligned} \tag{65}$$

Because $\rho_{\mathrm{ref}}(\mathbf{r})$ is a superposition of neutral atomic densities, the first two terms and the ion-ion repulsion, $v_{nn}(\mathbf{R})$, only depend on the atomic configuration, $\mathbf{R}$. We may therefore collect these three terms in a $\Delta\rho$-independent reference energy term,

$$E_{\mathrm{ref}}(\mathbf{R}) \equiv F[\rho_{\mathrm{ref}}] + \int v_{\mathrm{ext}}(\mathbf{R},\mathbf{r})\rho_{\mathrm{ref}}(\mathbf{r})\mathrm{d}\mathbf{r} + v_{nn}(\mathbf{R}). \tag{66}$$

We can then define a second-order DFTB energy expression of the electronic energy, $E_{\mathrm{DFTB}}(\mathbf{R},\rho)$, including the nuclear repulsion term, where

$$\begin{aligned} E_{\mathrm{DFTB}}(\mathbf{R},\rho) &= E_{\mathrm{ref}}(\mathbf{R}) \\ &+ \int \left(\frac{\delta F[\rho]}{\delta\rho}\bigg|_{\rho_{\mathrm{ref}}} + v_{\mathrm{ext}}(\mathbf{R},\mathbf{r}) \right) \Delta\rho(\mathbf{r})\mathrm{d}\mathbf{r} \\ &+ \frac{1}{2}\iint \Delta\rho(\mathbf{r})\,\frac{\delta^2 F[\rho]}{\delta\rho^2}\bigg|_{\rho_{\mathrm{ref}}} \Delta\rho(\mathbf{r'})\mathrm{d}\mathbf{r}\mathrm{d}\mathbf{r'}. \end{aligned} \tag{67}$$

This approximate energy expression forms the basis for second-order SCC-DFTB theory and it has several desirable properties that makes it easy to parameterize for fast and accurate electronic structure calculations. To use this second-order energy expression we first need to determine how to represent the electron density and then how to parameterize and approximate the different energy terms.

In any electronic structure calculation the net electron density must be positive, $\rho(\mathbf{r}) \geq 0$. This is a particularly important constraint in a variationally optimized formulation of the Born–Oppenheimer potential. The condition of a positive density can be met with an ansatz where the density, $\rho(\mathbf{r})$, is given as a sum of the square of normalized single-particle molecular orbitals, $\{\Psi_n(\mathbf{r})\}$, where

$$\begin{aligned} \rho(\mathbf{r}) &= 2\sum_{n=1}^{N_{\mathrm{occ}}} \rho_n(\mathbf{r}) = 2\sum_{n=1}^{N_{\mathrm{occ}}} \Psi_n^*(\mathbf{r})\Psi_n(\mathbf{r}), \\ \int \rho_n(\mathbf{r})\mathrm{d}\mathbf{r} &= \int \Psi_n^*(\mathbf{r})\Psi_n(\mathbf{r})\mathrm{d}\mathbf{r} = 1, \quad \forall n, \end{aligned} \tag{68}$$

for some general functions describing the normalized orbitals, $\{\Psi_n(\mathbf{r})\}$, and their corresponding single-electron densities, $\{\rho_n(\mathbf{r})\}$. The single-electron molecular orbitals allow a fine-grained description of the electronic structure that is aligned with well-established chemical intuition and provide an accurate kinetic energy expression in the Kohn–Sham formulation of the universal functional, $F[\rho]$. Notice, that we assume a spin-unpolarized system with double occupancy of each orbital, where N_{occ} is the number of occupied orbitals, which therefore is half the total number of electrons, N_e. Using some finite basis set, $\{\phi_i^{(n)}(\mathbf{r})\}_{i=1}^{N}$, of atom-centered functions we can then approximate each molecular orbital by

$$\Psi_n(\mathbf{r}) = \textstyle\sum_{i=1}^{N} c_i^{(n)}\phi_i^{(n)}(\mathbf{r}). \tag{69}$$

The positive electron density, $\rho(\mathbf{r}) \geq 0$, can then be generated in terms of these atom-centered functions using a density matrix representation, where

$$\begin{aligned} \rho(\mathbf{r}) &= 2\sum_{n=1}^{N_{\mathrm{occ}}} \Psi_n^*(\mathbf{r})\Psi_n(\mathbf{r}) \\ &= 2\left(\sum_{i=1}^{N} c_i^{(n)}\phi_i(\mathbf{r})\right)^* \left(\sum_{j=1}^{N} c_j^{(n)}\phi_j(\mathbf{r})\right) \\ &= 2\sum_{n=1}^{N_{\mathrm{occ}}}\sum_{i,j=1}^{N} (c_i^{(n)})^* c_j^{(n)}\phi_i^*(\mathbf{r})\phi_j(\mathbf{r}) \\ &= 2\sum_{n=1}^{N_{\mathrm{occ}}}\sum_{i,j=1}^{N} \varrho_{ij}^{(n)}\phi_i^*(\mathbf{r})\phi_j(\mathbf{r}) = 2\sum_{i,j=1}^{N} \varrho_{ij}\phi_i^*(\mathbf{r})\phi_j(\mathbf{r}). \end{aligned} \tag{70}$$

Here $\varrho_{ij} \equiv \sum_n (c_i^{(n)})^* c_j^{(n)}$ is the density matrix, $\boldsymbol{\varrho}$. We can use this density matrix formalism in Eq. (70), to represent the density difference, $\Delta\rho(\mathbf{r}) = \rho(\mathbf{r}) - \rho_{\text{ref}}(\mathbf{r})$, with the density matrix difference, $\Delta\boldsymbol{\varrho} = \boldsymbol{\varrho} - \boldsymbol{\varrho}_{\text{ref}}$, such that an underlying positivity in the net density automatically is enforced with $\rho(\mathbf{r}) \geq 0$. We can then write the second-order DFTB energy expression in Eq. (67) as a density matrix function,

$$E_{\text{DFTB}}(\mathbf{R}, \boldsymbol{\varrho}) = E_{\text{ref}}(\mathbf{R}) + 2\text{Tr}\left[\mathbf{H}^{(0)}\Delta\boldsymbol{\varrho}\right] + 2\text{Tr}\left[\Delta\boldsymbol{\varrho}\boldsymbol{\Gamma}^{\text{ref}}\Delta\boldsymbol{\varrho}\right], \tag{71}$$

where we use the tensor and matrix notation,

$$\begin{aligned}
\{\Gamma^{\text{ref}}\}_{ijkl} &= \iint \phi_i^*(\mathbf{r})\phi_j(\mathbf{r}) \left(\frac{\delta^2 F[\rho]}{\delta\rho(\mathbf{r'})\delta\rho(\mathbf{r})}\bigg|_{\rho_{\text{ref}}} \right) \\
&\quad \times \phi_k^*(\mathbf{r'})\phi_l(\mathbf{r}')\mathrm{d}\mathbf{r}\mathrm{d}\mathbf{r'}, \\
\{\boldsymbol{\Gamma}^{\text{ref}}\Delta\boldsymbol{\varrho}\}_{ij} &= \sum_{kl} \{\Gamma^{\text{ref}}\}_{ijkl}\Delta\varrho_{kl}, \\
H_{ij}^{(0)} &= \int \phi_i^*(\mathbf{r}) \left(\frac{\delta F[\rho]}{\delta\rho(\mathbf{r})}\bigg|_{\rho_{\text{ref}}} + v_{\text{ext}}(\mathbf{R},\mathbf{r}) \right) \phi_j(\mathbf{r})\mathrm{d}\mathbf{r}.
\end{aligned} \tag{72}$$

Here $\boldsymbol{\Gamma}^{\text{ref}}$ contains what can be referred to as the two-electron integrals. The functional derivatives are all evaluated at the reference density, i.e. at $\rho(\mathbf{r}) = \rho_{\text{ref}}(\mathbf{r})$, around which the second-order density expansions is performed. In SCC-DFTB we then use a Kohn–Sham energy expression for the universal functional, $F[\rho]$, where

$$\frac{\delta F[\rho]}{\delta\rho(\mathbf{r})} = -\frac{1}{2}\nabla^2 + \int \frac{\rho(\mathbf{r'})}{|\mathbf{r} - \mathbf{r}'|}\mathrm{d}\mathbf{r'} + V_{xc}[\rho](\mathbf{r}), \tag{73}$$

which uses an orbital-dependent kinetic energy term, a mean-field Hartree potential, and some approximation for the remaining exchange correlation potential, $V_{xc}[\rho](\mathbf{r}) = \delta E_{xc}[\rho]/\delta\rho(\mathbf{r})$. Here $E_{xc}[\rho]$ is the exchange-correlation energy functional for which various approximations are used [87,88]. In this case, the Hamiltonian matrix elements of $\mathbf{H}^{(0)}$ in Eq. (72) are given by

$$H_{ij}^{(0)} = \int \phi_i^*(\mathbf{r}) \left(-\frac{1}{2}\nabla^2 + \int \frac{\rho_{\text{ref}}(\mathbf{r'})}{|\mathbf{r}\text{-}\mathbf{r'}|}\mathrm{d}\mathbf{r'} + V_{xc}[\rho_{\text{ref}}] + v_{\text{ext}}(\mathbf{R},\mathbf{r}) \right) \phi_j(\mathbf{r})\mathrm{d}\mathbf{r}. \tag{74}$$

With the reference charge density of overlapping neutral atomic densities the external potential from the atomic nuclei, $v_{\text{ext}}(\mathbf{R},\mathbf{r})$, is screened already at a fairly short distance. In SCC-DFTB this screening is used to neglect three-center integrals, which allows an efficient two-center Slater–Koster parameterization of the Hamiltonian matrix elements of $\mathbf{H}^{(0)}$ [136]. This provides an efficient and accurate parameterization for off-diagonal blocks of the reference Kohn–Sham Hamiltonian matrix, $\mathbf{H}^{(0)}$. The diagonal on-site Hamiltonian matrix blocks are usually approximated by the diagonal atomic matrix components of the isolated neutral atoms, for which we assume the basis functions are close to their eigenstates. The same form of pairwise Slater–Koster parameterization is used also for the calculation of the overlap matrix, $S_{ij} = \langle\phi_i|\phi_j\rangle$. In this way each matrix element can be calculated at a speed similar to a classical local force field calculation.

In Kohn–Sham based SCC-DFTB theory we also approximate the two-electron Coulomb interaction term, including the exchange correlation, $E_{xc}[\rho]$, i.e. the term

$$\begin{aligned}
&2\text{Tr}\left[\Delta\boldsymbol{\varrho}\boldsymbol{\Gamma}^{\text{ref}}\Delta\boldsymbol{\varrho}\right] \\
&= \frac{1}{2}\iint \Delta\rho(\mathbf{r}) \left.\frac{\delta^2 F[\rho]}{\delta\rho(\mathbf{r'})\delta\rho(\mathbf{r})}\right|_{\rho_{\text{ref}}} \Delta\rho(\mathbf{r'})d\mathbf{r}d\mathbf{r'}, \\
&= \frac{1}{2}\iint \Delta\rho(\mathbf{r}) \left(\frac{1}{|\mathbf{r}\text{-}\mathbf{r'}|} + \left.\frac{\delta^2 E_{xc}[\rho]}{\delta\rho(\mathbf{r'})\delta\rho(\mathbf{r})}\right|_{\rho_{\text{ref}}} \right) \\
&\quad \times \Delta\rho(\mathbf{r'})d\mathbf{r}d\mathbf{r}',
\end{aligned} \tag{75}$$

using a monopole expansion over net Mulliken populations, $\{q_I\}$, for each atom, I, such that

$$\begin{aligned}
2\text{Tr}\left[\Delta\boldsymbol{\varrho}\boldsymbol{\Gamma}^{\text{ref}}\Delta\boldsymbol{\varrho}\right] &\approx \frac{1}{2}\sum_{IJ} q_I\gamma_{IJ}q_J \\
q_I &= 2\sum_{i\in I,j} \Delta\varrho_{ij}S_{ji},
\end{aligned} \tag{76}$$

where I, J indicate each atom with positions $\mathbf{R}_I$ and γ_{IJ} is a screened Coulomb interaction [136]. The summation over the orbital index $i \in I$ is performed only over orbitals centered at atom I, such that $\{q_I\}$ correspond to the net Mulliken charges. Higher order multipoles could also be used in a straightforward generalization [159]. The monopole interaction matrix, γ_{IJ}, captures the interaction of overlapping atomic charge densities, e.g. Gaussian charge distributions [130]. γ_{IJ} therefore decays as $1/|\mathbf{R}_I - \mathbf{R}_J|$ at large distances, but in the short-range limit it is screened and chosen to converge to the atomic Hubbard-U term for the onsite, γ_{II}, interactions corresponding to the chemical hardness.

The monopole approximation in Eq. (76) can alternatively be seen as a low-rank tensor approximation of the two-electron integral, where

$$\frac{1}{2}\sum_{IJ} q_I\gamma_{IJ}q_J = 2\sum_{IJ}\left(\sum_{i\in I,k;j\in J,l} \Delta\varrho_{ik}S_{ki}\gamma_{IJ}\Delta\varrho_{jl}S_{lj} \right), \tag{77}$$

which means that we represent the two-electron integral $\boldsymbol{\Gamma}^{\text{ref}}$ by

$$\Gamma_{ijkl}^{\text{ref}} \approx S_{ij}\gamma_{ik}S_{kl}, \tag{78}$$

where $\gamma_{ik} \equiv \gamma_{IK}$ when $i \in I$ and $k \in K$. Higher order multipole expansions for the approximation of the two-electron energy term would generate more accurate high-rank approximations. Alternative solutions based on the resolution of identity and other low-rank approximations could possibly also be applied. The tensor approximation of the two-electron integrals also indicates the direct coupling to semi-empirical Hartree–Fock theory and how, for example, an exchange term could be introduced by switching indices for the gamma term, $\Gamma_{ijkl} \rightarrow \Gamma_{ikjl}$.

With these approximations the DFTB energy approximation is

$$E_{\mathrm{DFTB}}(\mathbf{R}, \boldsymbol{\varrho}) = E_{\mathrm{ref}}(\mathbf{R}) + 2\mathrm{Tr}\left[\mathbf{H}^{(0)}\Delta\boldsymbol{\varrho}\right] + \frac{1}{2}\sum_{IJ} q_I \gamma_{IJ} q_J. \tag{79}$$

The remaining term that we need to represent in SCC-DFTB theory is the reference energy, $E_{\mathrm{ref}}(\mathbf{R})$, explicitly expressed in Eq. (66). For this term we may also include the Δ-charge independent reference energy term, $2\mathrm{Tr}[\mathbf{H}^{(0)}\boldsymbol{\varrho}_{\mathrm{ref}}]$, in $2\mathrm{Tr}[\mathbf{H}^{(0)}\Delta\boldsymbol{\varrho}] = 2\mathrm{Tr}[\mathbf{H}^{(0)}(\boldsymbol{\varrho} - \boldsymbol{\varrho}_{\mathrm{ref}})]$, or we may subtract the total energy of the non-interacting atoms such that $E_{\mathrm{ref}}(\mathbf{R})$ corresponds to the formation energy. No matter which choice we make, $E_{\mathrm{ref}}(\mathbf{R})$ is typically used as an adjustable charge-independent energy term for which we can use different parameterizations, e.g. pair or many-body potentials, and optimizations based on data from first-principles electronic structure calculations [33,135,136,147,160,161].

Using the orbital-based Kohn–Sham density functional expression, the Slater–Koster parameterization of the matrix elements for $\mathbf{H}^{(0)}$ and the overlap matrix in combination with the monopole approximation for the two-electron integral, and the parameterization of the reference energy, we arrive at the regular formulation of second-order SCC-DFTB theory. For this level of theory the Born–Oppenheimer potential energy is given from the constrained minimization over the charge fluctuations,

$$U_{\mathrm{DFTB}}(\mathbf{R}) = E_{\mathrm{ref}}(\mathbf{R}) + \min_{\Delta\boldsymbol{\varrho}}\left\{2\mathrm{Tr}\left[\mathbf{H}^{(0)}_{\mathrm{KS}}\Delta\boldsymbol{\varrho}\right] + \frac{1}{2}\sum_{IJ} q_I\gamma_{IJ}q_J \,\middle|\, \mathrm{Tr}\left[\boldsymbol{\varrho}_n\mathbf{S}\right] = 1\right\}. \tag{80}$$

The minimization is achieved by solving the non-linear eigenvalue problem

$$\mathbf{H}\mathbf{c}_n = \epsilon_n\mathbf{S}\mathbf{c}_n, \quad n = 1, 2, \ldots, N_{\mathrm{occ}}, \tag{81}$$

where

$$\mathbf{H} = \mathbf{H}^{\mathrm{ref}}_{\mathrm{KS}} + \frac{1}{2}\left(\mathbf{V}_{\mathrm{C}}\mathbf{S} + \mathbf{S}\mathbf{V}_{\mathrm{C}}\right),$$

$$\{\mathbf{V}_{\mathrm{C}}\}_{ij} = \delta_{i,j} \times \sum_J \gamma_{IJ}q_J, \ \forall i,j \in I$$
$$\boldsymbol{\varrho} = \sum_n \mathbf{c}_n\mathbf{c}_n^T, \quad \rho(\mathbf{r}) = 2\sum_{ij}\varrho_{ij}\phi_i^*(\mathbf{r})\phi_j(\mathbf{r}),$$
$$q_I = 2\sum_{i\in I,j}\Delta\varrho_{ij}S_{ji} = 2\sum_{i\in I,j}(\varrho_{ij} - \varrho^{\mathrm{ref}}_{ij})S_{ji}. \tag{82}$$

Here $\mathbf{V}_{\mathrm{C}}$ is a diagonal Coulomb matrix with different values for each atomic site, but which is equal for each orbital on any given atomic site.

It is interesting to note that the $\frac{1}{2}(\mathbf{V}_{\mathrm{C}}\mathbf{S} + \mathbf{S}\mathbf{V}_{\mathrm{C}})$ term in Eq. (82) can be seen as a trapezoidal-like integral approximation of three-center integrals that arise from the electrostatic potential of distant atoms with net Mulliken charges. For the reference system of overlapping neutral atoms densities, these long-range contributions are not present.

5.2 XL-BOMD for SCC-DFTB

To construct an XL-BOMD based on SCC-DFTB theory we can view the DFTB energy expression, $E_{\mathrm{DFTB}}(\mathbf{R}, \boldsymbol{\varrho})$ in Eq. (79), as a density matrix function and design an approximate shadow potential using a linearization around an approximate ground-state density matrix, in the same way as we did for Hartree–Fock theory in Eq. (56). However, this is not the most efficient way of constructing a shadow Born–Oppenheimer potential for XL-BOMD. Instead of the density matrix, we can use the net Mulliken charges, $\mathbf{q} = \{q_I\}$, that indirectly define the effective single-particle Hamiltonian, $\mathbf{H}$ in Eq. (82), and therefore also the relaxed ground state solution, $\Delta\boldsymbol{\varrho}_{\mathrm{min}}$, which minimizes the energy for the Born–Oppenheimer potential in Eq. (80). The corresponding ground state net Mulliken charges are $\mathbf{q}_{\mathrm{min}} = \{q_I^{\mathrm{min}}\}$. Our choice of approximate shadow energy functional, $\mathcal{E}_{\mathrm{DFTB}}(\mathbf{R}, \mathbf{q}, \mathbf{n}) \approx E_{\mathrm{DFTB}}(\mathbf{R}, \boldsymbol{\varrho})$, is then given from a linearization of $E_{\mathrm{DFTB}}(\mathbf{R}, \boldsymbol{\varrho})$ in Eq. (79) around an approximate set of net Mulliken charges, $\mathbf{n} \approx \mathbf{q}_{\mathrm{min}}$, where

$$\mathcal{E}_{\mathrm{DFTB}}(\mathbf{R}, \mathbf{q}, \mathbf{n}) = E_{\mathrm{ref}}(\mathbf{R}) + 2\mathrm{Tr}\left[\mathbf{H}^{(0)}_{\mathrm{KS}}\Delta\boldsymbol{\varrho}\right] + \frac{1}{2}\sum_{IJ}(2q_I - n_I)\gamma_{IJ}n_J. \tag{83}$$

The corresponding $\mathbf{n}$-dependent shadow Born–Oppenheimer potential is then

$$\mathcal{U}_{\mathrm{DFTB}}(\mathbf{R},\mathbf{n}) = E_{\mathrm{ref}}(\mathbf{R}) + \min_{\mathbf{q}}\left\{2\mathrm{Tr}\left[\mathbf{H}^{(0)}_{\mathrm{KS}}\Delta\boldsymbol{\varrho}\right] + \frac{1}{2}\sum_{IJ}(2q_I - n_I)\gamma_{IJ}n_J \,\middle|\, \mathrm{Tr}\left[\boldsymbol{\varrho}_n\mathbf{S}\right] = 1\right\}, \tag{84}$$

with the optimized charges, $\mathbf{q}_0[\mathbf{n}]$, attained at the lowest stationary solution,

$$\mathbf{q}_0[\mathbf{n}] = \arg\min_{\mathbf{q}} \left\{ 2\mathrm{Tr}\left[\mathbf{H}^{(0)}_{\mathrm{KS}} \Delta\boldsymbol{\varrho}\right] + \frac{1}{2}\sum_{IJ}(2q_I - n_I)\gamma_{IJ}n_J \;\middle|\; \mathrm{Tr}\left[\boldsymbol{\varrho}_n \mathbf{S}\right] = 1 \right\}. \tag{85}$$

We can then construct our XL-BOMD by defining the extended Lagrangian

$$\mathcal{L}_{\mathrm{XBO}}(\mathbf{R}, \dot{\mathbf{R}}, n, \dot{n}) = \frac{1}{2}\sum_I M_I |\dot{\mathbf{R}}_I|^2 - \mathcal{U}_{\mathrm{DFTB}}(\mathbf{R},\mathbf{n}) + \frac{1}{2}\mu\sum_I \dot{n}_I^2 - \frac{1}{2}\mu\omega^2 \sum_{IJ}(q_{0I}[\mathbf{n}] - n_I)\, T_{IJ}\, (q_{0J}[\mathbf{n}] - n_J)\,, \tag{86}$$

where the evolution of the dynamical variable charges, $\mathbf{n}(t)$, is driven by a harmonic oscillator centered around the optimized charges, $\mathbf{q}_0[\mathbf{n}]$, for the shadow Born–Oppenheimer potential. As discussed previously, the matrix, $\mathbf{T} = \mathbf{K}^T\mathbf{K} = \{T_{IJ}\}$, is a metric tensor that is given by the kernel, $\mathbf{K}$, which is defined as the inverse of the Jacobian, $\mathbf{J}$, of the residual function, $\mathbf{f(n)} = \mathbf{q}_0[\mathbf{n}] - \mathbf{n}$, i.e.

$$J_{IJ} = \frac{\partial f_I(\mathbf{n})}{\partial n_J}, \qquad \mathbf{K} = \mathbf{J}^{-1}. \tag{87}$$

In the same way as before, μ is also a fictitious electron mass parameters and ω is the frequency of the extended harmonic oscillator.

In the adiabatic limit as $\mu \to 0$ and $\omega \to \infty$ such that $\mu\omega =$ constant, Euler–Lagrange equations give us the equations of motion,

$$M_I \ddot{\mathbf{R}}_I = -\nabla_{\mathbf{R}_I} \mathcal{U}_{\mathrm{DFTB}}(\mathbf{R},\mathbf{n})|_{\mathbf{n}}\,, \qquad \ddot{\mathbf{n}} = -\omega^2 \mathbf{K}\left(\mathbf{q}_0[\mathbf{n}] - \mathbf{n}\right). \tag{88}$$

The corresponding constant of motion is

$$E^{\mathrm{DFTB}}_{\mathrm{XBO}} = \tfrac{1}{2}\textstyle\sum_I M_I |\dot{\mathbf{R}}_I|^2 + \mathcal{U}_{\mathrm{DFTB}}(\mathbf{R}, \mathbf{n}). \tag{89}$$

The presentation above does not account for fractional occupation numbers or the corresponding entropy term, but these can be included in the same way as for thermal Hartree–Fock theory. This is of particular importance if we simulate degenerate systems or systems with charge sloshing and metals. A demonstration of such a system is given in the example below.

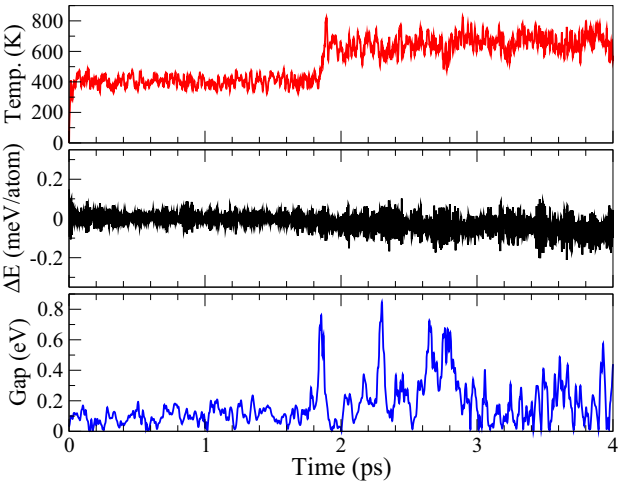

Fig. 6 XL-BOMD simulations of amorphous carbon (55 atoms with periodic boundary conditions) based on SCC-DFTB theory. Fractional occupation numbers corresponding to an electronic temperature of 500 K was used. The integration time step was 0.75 fs. The upper panel shows the statistical temperature, the middle panel the fluctuations in the total energy, and the lower panel shows the electronic gap corresponding to the HOMO-LUMO gap for integer occupation numbers at a zero electronic temperature

5.3 Example

One of the more challenging forms of QMD simulations is for reactive systems, where the electronic gap is opening and closing along the molecular trajectories. Amorphous carbon is an example with this behavior. Figure 6 shows the results of an XL-BOMD simulation based on SCC-DFTB theory [28,135,162], including fractional occupation numbers, which also is using the preconditioned Krylov subspace approximation of the Kernel in the integration of the electronic degrees of freedom that are represented by the net Mulliken charges [28]. The system starts from a non-equilibrium configuration with stationary carbon atoms. Initially, the statistical temperature is rapidly increasing to about 400 K during the first 100 fs, shown in the upper panel, while the electronic gap, shown in the lower panel, is opening and closing. Shortly before 2 ps there is an exothermic reaction noticed in a rapid increase in the temperature and decrease in the gap. The increased temperature is also noticed in an increased amplitude of the fluctuations in the total energy, shown in the mid panel.

6 XL-BOMD for a non-linear charge relaxation model

If we apply XL-BOMD to orbital-independent models such as polarizable force fields or charge relaxation models [59–62,163–172] we need a modified formulation from the orbital-based models discussed above [30]. In particular, instead of performing a linearization of the

energy functional around some approximate density, $n(\mathbf{r})$, we perform a mixed expansion, which is possible with the more general shadow functional definition in Eq. (8). The energy functional is expanded to second order around $n(\mathbf{r})$ for diagonal on-site charge energy terms and to first order for all other terms including the long-range Coulomb interaction energy. The theory was recently developed and presented in some detail in Ref. [30]. To demonstrate how this works we use the general non-linear monopole charge relaxation model,

$$E(\mathbf{R},\mathbf{q}) = V(\mathbf{R}) + E_{\mathrm{s}}(\mathbf{R},\mathbf{q}) + \frac{1}{2}\sum_{i,j(i\neq j)} q_i \gamma_{ij}(\mathbf{R}) q_j, \quad (90)$$

where $E_{\mathrm{s}}(\mathbf{R},\mathbf{q})$ is some non-linear charge-dependent energy term, but only with short-range (s) interactions between atom-centered net monopole charges, $\mathbf{q} = \{q_i\}$, for each atom i. All the long-range interactions are instead included through the Coulomb interaction between atom centered net charge densities, which is governed by the screened Coulomb interaction terms, $\{\gamma_{ij}\} \equiv \boldsymbol{\gamma}(\mathbf{R})$. The $V(\mathbf{R})$ is a charge independent interaction term, which is included separately from $E_{\mathrm{s}}(\mathbf{R},\mathbf{q})$ because it may also include long-range interactions. Generalization to more flexible atom-centered charges, besides the atomic net monopole charges are straightforward, including dipoles and quadrupoles, at least in principle [30]. In this case $\mathbf{q}$ in $E(\mathbf{R},\mathbf{q})$ would represent a vector that also contains the higher order multipoles and $\gamma_{ij}(\mathbf{R})$ would represent the long-range monopole-monopole, dipole-monopole, dipole–dipole, and monopole-quadrupole interactions or higher order terms. Van der Waals interactions can also be included separately to the energy expression in Eq. (90). The discussion below is only focused on monopole charges, but should follow analogous for higher order multipole moments and Van der Waals interactions. The charge relaxation models represented by $E(\mathbf{R},\mathbf{q})$ in Eq. (90) could potentially be constructed and optimized using machine-learning based on pre-calculated data using high-level ab initio theory [142,144,173]. Alternatively, we can derive the expression for $E(\mathbf{R},\mathbf{q})$ from Hohenberg–Kohn DFT using an expansion of the DFT functional around overlapping neutral atomic densities and a density tight-binding approximation that represents the local atomic deformations [30]. Other simplified charge equilibration models can also be used [30,142,164,165,171,173].

The Born–Oppenheimer potential energy surface, $U_{\mathrm{BO}}(\mathbf{R})$, and the relaxed ground state charges, $\mathbf{q}_{\mathrm{min}}$, determined by the monopole charge relaxation model in Eq. (90) are given by the constrained non-linear optimizations,

$$U_{\mathrm{BO}}(\mathbf{R}) = \min_{\mathbf{q}} \left\{ E(\mathbf{R},\mathbf{q}) \;\middle|\; \sum_{i\in\alpha} q_i = Q_\alpha \right\},$$
$$\mathbf{q}_{\mathrm{min}} = \arg\min_{\mathbf{q}} \left\{ E(\mathbf{R},\mathbf{q}) \;\middle|\; \sum_{i\in\alpha} q_i = Q_\alpha \right\}. \quad (91)$$

We have here introduced multiple charge constraints for different parts, $\{\alpha\}$, of the system. The charges Q_α can be identified, for example, as the net charge of separate fragments, α, that may form during an MD simulation. If no overlap to other fragments exists, we may assume that the net charge of each fragment, α, is conserved, which can be enforced by Lagrangian multipliers, $\{\lambda_\alpha\}$. The constrained optimization requires a solution of a system of non-linear equations,

$$\frac{\partial E(\mathbf{R},\mathbf{q})}{\partial q_i} = 0,$$
$$\sum_{i\in\alpha} q_i = Q_\alpha, \quad \alpha = a,b,\ldots, \quad (92)$$

which can be solved, for example, using some iterative Newton based scheme. This is computationally expensive and similar in complexity to the non-linear eigenvalue equation in orbital-based electronic structure theory.

An XL-BOMD based on the charge relaxation model can be designed by first constructing an approximate shadow functional, $\mathcal{E}(\mathbf{R},\mathbf{q},\mathbf{n}) \approx E(\mathbf{R},\mathbf{q})$, that is close to the energy functional in Eq. (90). If $\mathbf{n} \approx \mathbf{q}_{\mathrm{min}}$, we may define this shadow functional by a mixed expansion,

$$\begin{aligned}\mathcal{E}(\mathbf{R},\mathbf{q},\mathbf{n}) = {} & V(\mathbf{R}) + E_{\mathrm{s}}(\mathbf{R},\mathbf{n}) \\ & + \sum_i (q_i - n_i) \left.\frac{\partial E_{\mathrm{s}}(\mathbf{R},\mathbf{q})}{\partial q_i}\right|_{\mathbf{n}} \\ & + \frac{1}{2}\sum_i (q_i - n_i)^2 \left.\frac{\partial^2 E_{\mathrm{s}}(\mathbf{R},\mathbf{q})}{\partial q_i^2}\right|_{\mathbf{n}} \\ & + \frac{1}{2}\sum_{i,j(i\neq j)} (2q_i - n_i)\gamma_{ij} n_j, \end{aligned} \quad (93)$$

where we only expand the diagonal part of the short-range energy term to second order. All other terms are expanded only to linear order in (**q** - **n**). The corresponding shadow Born–Oppenheimer potential energy surface and the relaxed charges are then given from the constrained linear optimizations,

$$\mathcal{U}_{\mathrm{BO}}(\mathbf{R},\mathbf{n}) = \min_q \left\{ \mathcal{E}(\mathbf{R},\mathbf{q},\mathbf{n}) \;\middle|\; \sum_{i\in\alpha} q_i = Q_\alpha \right\},$$
$$\mathbf{q}_0[\mathbf{n}] = \arg\min_q \left\{ \mathcal{E}(\mathbf{R},\mathbf{q},\mathbf{n}) \;\middle|\; \sum_{i\in\alpha} q_i = Q_\alpha \right\}, \quad (94)$$

where we search for the lowest stationary solutions. The charge constraints can be included through Lagrangian multipliers. Assuming we have two net charge constrains, where $q_1 + q_2 = Q_a$ and $q_3 + q_4 + \ldots + q_N = Q_b$, the relaxed charge equilibrium is given by the solution

to the quasi-diagonal linear system of equations,

$$\begin{bmatrix} \Lambda_{11} & 0 & 0 & \dots & 0 & -1 & 0 \\ 0 & \Lambda_{22} & 0 & \dots & 0 & -1 & 0 \\ 0 & 0 & \Lambda_{33} & \dots & 0 & 0 & -1 \\ \vdots & \vdots & \vdots & \ddots & \vdots & \vdots & \vdots \\ 0 & 0 & 0 & \dots & \Lambda_{NN} & 0 & -1 \\ 1 & 1 & 0 & \dots & 0 & 0 & 0 \\ 0 & 0 & 1 & \dots & 1 & 0 & 0 \end{bmatrix} \begin{bmatrix} q_{01} \\ q_{02} \\ q_{03} \\ \vdots \\ q_{0N} \\ \lambda_1 \\ \lambda_2 \end{bmatrix} = \begin{bmatrix} v_1 \\ v_2 \\ v_3 \\ \vdots \\ v_N \\ Q_a \\ Q_b \end{bmatrix}, \tag{95}$$

where

$$\Lambda_{ii} = \left.\frac{\partial^2 E_{\mathrm{s}}(\mathbf{R},\mathbf{q})}{\partial q_i^2}\right|_{\mathbf{n}},$$
$$v_i \equiv v_i[\mathbf{n}] = \Lambda_{ii} n_i - \sum_{j\neq i} \gamma_{ij} n_j - \left.\frac{\partial E_{\mathrm{s}}(\mathbf{R},\mathbf{q})}{\partial q_i}\right|_{\mathbf{n}}. \tag{96}$$

This system of linear equations has a trivial analytical solution,

$$\lambda_\alpha = \left(Q_\alpha - \sum_{i\in\alpha} v_i \Lambda_{ii}^{-1}\right)\left(\sum_{i\in\alpha} \Lambda_{ii}^{-1}\right)^{-1},$$
$$q_{0i}[\mathbf{n}] = \Lambda_{ii}^{-1}(\lambda_\alpha + v_i), \quad i \in \alpha. \tag{97}$$

The difference in the computational cost to solve the full non-linear system of equations in Eq. (92) compared to the straightforward analytical solution in Eq. (97) is therefore significant, in particular for larger systems with maybe tens of thousands of atoms.

The shadow Born–Oppenheimer potential, $\mathcal{U}_{\mathrm{BO}}(\mathbf{R},\mathbf{n})$, can then be used in an extended Lagrangian formulation, where $\mathbf{n}$ is included as a dynamical vector variable,

$$\mathcal{L}(\mathbf{R},\dot{\mathbf{R}},n,\dot{n}) = \frac{1}{2}\sum_i M_i|\dot{\mathbf{R}}_i|^2 - \mathcal{U}_{\mathrm{BO}}(\mathbf{R},\mathbf{n}),$$
$$+\frac{\mu}{2}\sum_i \dot{n}_i^2 - \frac{\mu\omega^2}{2}(\mathbf{q}_0[\mathbf{n}]-\mathbf{n})^T\mathbf{T}(\mathbf{q}_0[\mathbf{n}]-\mathbf{n}), \tag{98}$$

in the same way as for orbital-dependent XL-BOMD. Here $\mathbf{T} = \mathbf{K}^T\mathbf{K}$ is a metric tensor, μ is the fictitious mass parameter of the electronic degrees of freedom and ω is the frequency of the extended harmonic oscillator. We can then derive the equations and constant of motion in the adiabatic limit, which defines the XL-BOMD for the charge relaxation model in Eq. (93). For this adiabatic limit the $\sim 1/\omega^2$ scaling is important such that

$$\frac{\partial\mathcal{E}(\mathbf{r},\mathbf{q},\mathbf{n})}{\partial\mathbf{n}} \propto |\mathbf{q}\text{ - }\mathbf{n}| \propto \omega^{-2}, \tag{99}$$

which is fulfilled by $\mathcal{E}(\mathbf{r},\mathbf{q},\mathbf{n})$ in Eq. (93). In the adiabatic limit, as $\omega \to \infty$ and $\mu \to 0$ such that $\mu\omega =$ constant, the Euler–Lagrange equations of motion are given by

$$M_i\ddot{\mathbf{R}}_i = -\nabla_{\mathbf{R}_i}\mathcal{U}_{\mathrm{BO}}(\mathbf{R},\mathbf{n})|_{\mathbf{n}},$$
$$\ddot{\mathbf{n}} = -\omega^2\mathbf{K}(\mathbf{q}_0[\mathbf{n}]-\mathbf{n}). \tag{100}$$

The kernel, $\mathbf{K}$, can be calculated from the inverse Jacobian of the residual function, $\mathbf{f}(\mathbf{n}) = (\mathbf{q}_0[\mathbf{n}]-\mathbf{n})$, where $\mathbf{q}_0[\mathbf{n}]$ is given from $\mathbf{n}$ by the linear relation in Eq. (97) [30]. The integration can then be performed as in Eq. (20).

6.1 Example

A simplified example of the more general non-linear charge relaxation model in Eq. (90) is the charge equilibration model by Rappe and Goddard [165], where

$$E(\mathbf{R},\mathbf{q}) = V(\mathbf{R}) + \sum_i \chi_i q_i + \frac{1}{2}\sum_i q_i^2 U_i$$
$$+\frac{1}{2}\sum_{i,j(i\neq j)} q_i\gamma_{ij}(\mathbf{R})q_j. \tag{101}$$

The short-ranged energy term in Eq. (90) is here replaced by a linear term in the energy as a function of the net charge on each atom with $\{\chi_i\}$ determined by the atomic electronegativities and a quadratic term, where $\{U_i\}$ correspond to the chemical hardness or Hubbard-U parameters. The corresponding shadow energy function becomes,

$$\mathcal{E}(\mathbf{R},\mathbf{q},\mathbf{n}) = V(\mathbf{R}) + \sum_i \chi_i q_i + \frac{1}{2}\sum_i q_i^2 U_i$$
$$+\frac{1}{2}\sum_{i,j(i\neq j)} (2q_i - n_i)\gamma_{ij}(\mathbf{R})n_j, \tag{102}$$

where the vector for the net atomic charges, $\mathbf{n}(t)$, is used as a dynamical vector variable in the extended Lagrangian formulation in Eq. (98). The the equilibrated charges and the Born–Oppenheimer potential energy surface are then given from the solution of a quasi-diagonal, linear system of equations as in Eq. (95).

A demonstration of an XL-BOMD simulation based on the charge equilibration model in Eq. (102) with periodic boundary conditions is shown in Fig. 7 for a simple three-atom molecular system, with the atomic masses corresponding to oxygen and two hydrogen atoms (where one of the hydrogen atoms has an extra neutron). The electronegativities, $\{\chi_i\}$, the chemical hardness or Hubbard-U parameters, $\{U_i\}$, and the charge-independent interatomic potential, $V(\mathbf{R})$, were not optimized for water. The three-atom system is

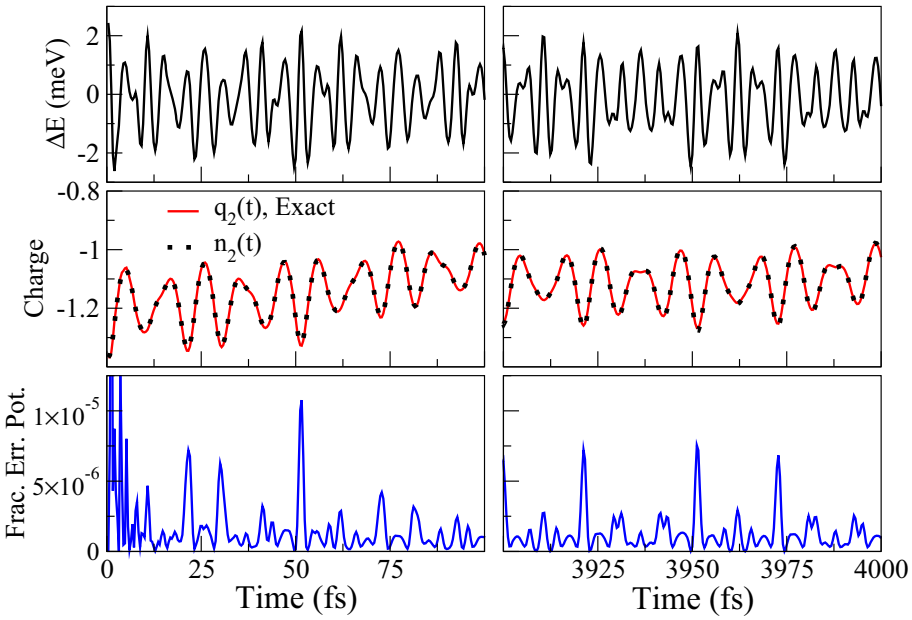

Fig. 7 XL-BOMD simulations for a water-like molecule in a 5 Å cubic box with periodic boundary conditions described by the charge equilibrium model in Eq. (101). The time step was set to 0.4 fs. The left-side panels show the initial part of the simulation and the right-hand panels show the results after about 4 ps of simulation time. The upper panels show the fluctuations in the total energy, the middle panels the fluctuations in the dynamical charge, $n_q(t)$, for the "oxygen" atom in comparison to its exact Born–Oppenheimer charge, $q_2(t)$, in each time step. The lower panels show the fractional error in the potential energy, $|\mathcal{U}_{\mathrm{BO}}(t) - U_{\mathrm{BO}}(t)|/U_{\mathrm{BO}}(t)$, in comparison to the exact Born–Oppenheimer potential, $U_{\mathrm{BO}}(t)$, in each time step. The sampling of the Born–Oppenheimer potential energy surface is virtually exact

therefore only a water-like molecule. The modified Verlet scheme in Eq. (20) was used to integrate the equations of motion together with a fixed constant kernel [30]. The left panels shows the initial part of the simulation, whereas the panels on the right-hand side show the results after about 4 ps of simulation time. The error in the charges (mid panels) and in the sampling of the potential energy surface (bottom panels) are negligible without any visible drift in total energy (upper panel).

The ability to perform MD simulations for charge equilibration models without repeated Coulomb summations in each time step provides a significant acceleration. This is of particular interest to the application of modern machine learning tools that show an exceptional promise in the accurate parametrization of short-range interatomic potentials. A remaining challenge however, is to include long-range force terms governed by the Coulomb interactions and the corresponding charge relaxations, without a drastic increase in the computational cost. XL-BOMD provides an approach to avoid this potential shortcoming as demonstrated in Fig. 7.

7 Applications

Various forms of XL-BOMD have been used in a number of software packages, including density functional theory, semi-empirical electronic structure theory, polarizable force fields, excited state dynamics, and superfluidity [16,17,20,21,23,27,32,33,33–49]. A few of those will be discussed below. However, most applications have so far been focused on earlier versions of XL-BOMD and do not take full advantage of the shadow Born–Oppenheimer potential and the equations of motion in the full adiabatic limit that is achieved with the generalized metric tensor of the harmonic oscillator extension. Some XL-BOMD applications to industrial problems with focus on linear scaling methods was recently presented in Ref. [31].

7.1 Improving QMD in electronic structure codes

XL-BOMD, both in its earlier form of time-reversible Born–Oppenheimer MD and in its shadow Lagrangian formulation presented here, can be used to accelerate quantum-based Born–Oppenheimer simulations. As such it has been implemented in electronic structure codes, including FreeON [174,175], TeraChem [36], LATTE [162], SCC-DFTB [16,33,37], UQuantChem [35], ONETEP [38,176], CONQUEST [20,41,177], NEXMD [178], and PYSEQM [49].

7.2 Linear scaling electronic structure theory

Linear scaling electronic structure theory uses approximate solvers that avoid the full diagonalization of the quantum mechanical eigenvalue problem, which has a computational cost that scales cubically with the sys-

tem size. Instead, divide and conquer approaches or numerically thresholded sparse matrix algebra techniques are used [179,180]. With these techniques the computational complexity can be reduced such that the computational cost only increases linearly with the system size. A major problem with linear scaling electronic structure theory is the ability to reach a sufficiently high degree of SCF convergence. Attempts to achieve linear scaling complexity in combination with QMD simulations have, therefore, often lead to significant drifts in the total energy because of an underlying broken time-reversal symmetry [181–184]. XL-BOMD avoids this systematic drift and makes it possible to achieve stable energy conserving, linear scaling Born–Oppenheimer molecular dynamics simulations [17,20,25,31,38,41,185,186].

7.3 Thermostated XL-BOMD

A main shortcoming of regular Born–Oppenheimer MD simulations is the systematic drift in the total energy if we combine an electronic extrapolation from previous ground state solutions as an initial guess to the SCF optimization with an incomplete convergence. But, what happens when we go beyond microcanonical NVE simulations? For example, if we perform canonical simulations with thermostats, where we rescale the velocities or apply random noise to the forces as in a Langevin dynamics, then the total energy is not even conserved and we may expect that the original problem might simply disappear. In applications of XL-BOMD to canonical QMD simulations, we find that even if the total energy is not conserved, properties such as the distribution of the thermal fluctuations are of key importance [103]. Without tightly converged forces in regular direct Born–Oppenheimer MD, the thermal fluctuations are unphysical. Properties such as diffusion, the heat capacity, the thermal conductivity, or the frequency of rare events, will therefore not be represented correctly. With thermostated XL-BOMD it can be demonstrated that these shortcomings are avoided [41,103].

7.4 Reactive unstable systems

If a system has SCF instabilities with charge sloshing or a closed degenerate HOMO-LUMO gap, any form of Born–Oppenheimer molecular dynamics simulations may run into problems. This is also the case for XL-BOMD. A simple scaled delta-function approximation of the kernel in the electronic equations of motion is no longer possible and fractional occupation numbers have to be included to account for degenerate states if the HOMO-LUMO gap is closing. With the generalization of XL-BOMD that includes the electronic free-energy and preconditioned Krylov subspace approximations of the kernel with adaptive rank-m updates [26,28,29,32], it is possible to treat systems that normally would be very challenging, as was illustrated by the example in Fig. 6.

7.5 Excited states

An extended Lagrangian formulations for time-dependent self-consistent field theory is also possible [27]. In this case we can dynamically propagate transition matrices that describe the excited states in combination with the evolution of the electronic ground state. The molecular trajectories are then generated by interatomic forces that are determined by the excited state potential energy surface. However, so far, this extended Lagrangian approach has not been able to take full advantage of the most recent formulations of XL-BOMD, but the speedup can still be significant [27].

7.6 Superfluidity

The application to time-dependent self-consistent field theory can also be extended to superfluidity [46], where the shadow energy functional is replaced by a shadow Lagrangian that represents a time-dependent non-linear Schrödinger-like equation, such as the Gross–Pitaevskii equation. The shadow Lagrangian formulation leads to two coupled equations that both are linear in their time-derivative variables. This allows the application of efficient and stable implicit time integration schemes, without having to solve a non-linear equation in each time step.

7.7 Charge equilibration and polarizable field models

Polarizable force fields and charge equilibration models are frequently used to study a broad range of materials—in particular bio-molecular systems. These models can be derived as coarse grained formulations of orbital-free DFT, where the electron density are described by atom-centered charge deformations that are approximated by multipoles. Because of the long-range (all-to-all) electrostatic interactions, the dipole or charge relaxations require the solution of a full dense linear system of equations. These systems often require iterative solvers, in particular for systems with periodic boundary conditions. The iterative solution then plays a similar role to the SCF optimization procedure in orbital-based electronic structure calculations. By propagating an approximate solution represented by extended dynamical variables, a broken time-reversibility and a systematic energy drift can be avoided, even with approximately converged solutions in each time step [23,24,38,43–45,108]. This gives a significant reduction of the computational cost. Recently, it was possible to formulate XL-BOMD in its most recent framework, with features previously only applicable to orbital-based XL-BOMD, also for these orbital-free models [30]. These features, as discussed above, include the metric tensor generalization of the extended harmonic potential, preconditioners, and the ability to use only a single Coulomb summation to determine the fully equilibrated charges and the interatomic forces in each time step for the shadow Born–Oppenheimer

potential energy surface. An example was demonstrated in Fig. 7.

8 Summary and outlook

In this brief review we have presented XL-BOMD for various levels of electronic structure theory, from Hohenberg–Kohn density functional theory to coarse grained charge relaxation models. XL-BOMD appears as a general framework that can be adapted and applied to a broad variety of electronic structure models. Computationally efficient and accurate trajectories are generated by propagating extended electronic degrees of freedom, in the spirit of Car–Parrinello MD, through a harmonic oscillator that is centered around an optimized electronic ground state, in combination with an approximate shadow energy functional that is linearized around the extended electronic degrees of freedom. No iterative solvers are needed to find the electronic ground state and only a single Coulomb summation is required to find the fully equilibrated charges in each time step. The framework of XL-BOMD therefore provides a significant boost to a broad variety of molecular dynamics simulation methods based on a number of underlying models for the electronic structure.

In this review we have tried to be pedagogical by explaining the electronic structure models and how they can be formulated in the framework of XL-BOMD. The different examples hopefully help the reader understand the theory and show how XL-BOMD can be applied also to other models not discussed here. For some of the more technical details we sometimes may have been fairly brief, but the reader can then consult the original publications or other literature.

A major part of existing implementations and applications are currently based on early versions of XL-BOMD that cannot take full advantage of the most recent formulation, including efficient preconditioners and an exact ground state optimization of a linearized functional with SCF-free equations of motion that are derived in an adiabatic mass-zero limit. Using the updated framework of XL-BOMD could provide a significant boost to current implementations—improve stability, allow slightly longer integration time steps, and completely remove the need for any iterative SCF optimization.

Despite the recent progress in the development of XL-BOMD, there is plenty of room for improvements and new applications. A few missing ingredients include, for example: (1) a preconditioner for the density matrix formulation of XL-BOMD; (2) more rigorous and less ad hoc integration schemes for a variety of ensembles; (3) implementations in a variety of state-of-the art ab initio electronic structure codes; (4) applications of XL-BOMD for the non-linear charge relaxation models that are parameterized and optimized using modern machine learning methods; (5) linear scaling implementations of XL-BOMD for fractional occupation numbers including the low-rank Krylov subspace approximation of the kernels; and (6) a careful mathematical analysis of stability and efficiency of XL-BOMD for different electronic structure models and ensembles.

XL-BOMD provides a theoretical framework that relies on a physics-based reformulation of the underlying Born–Oppenheimer dynamics. This reformulation makes it possible to avoid the cumbersome solution of a non-linear eigenvalue problem or a dense system of equations. Instead, only a simplified linear eigenvalue problem has to be solved for the orbital-based models or a quasi-diagonal system of equations for the non-linear charge relaxation models. This represents an example of the value of a coordinated design approach. To optimize software implementations and to improve hardware or the parallelism for hybrid architectures are all important if we want to enhance the computational efficiency, but it is only a genuinely cross-disciplinary approach, where we also reformulate the underlying physics, which allows a truly transformative step forward. This may, of course, sound like an obvious statement to many scientists, but yet it is frequently forgotten.

Acknowledgements The author is indebted and grateful to a number of collaborators that have contributed to the development of XL-BOMD during the last decade of which most appear as co-authors of the XL-BOMD publications cited in this review. Some of those that do not appear as co-authors, but still have contributed through stimulating discussions and critical comments are Eric Chisolm, Jürg Hutter, Travis Peery, Kipton Barros, Linnea Andersson, Joshua Finkelstein, Vikram Gavini, Konstantin Leon, Mariana Rossi, Oscar Gråsäs, Anders Bergman, and John Wills. This work is supported by the U.S. Department of Energy Office of Basic Energy Sciences ("Next generation quantum based molecular dynamics", FWP LANLE8AN / KC0301061) and by the U.S. Department of Energy through the Los Alamos National Laboratory. Los Alamos National Laboratory is operated by Triad National Security, LLC, for the National Nuclear Security Administration of the U.S. Department of Energy Contract No. 892333218NCA000001.

Data Availability Statement This manuscript has no associated data or the data will not be deposited. [Authors' comment: Additional data or information can be made available by the author upon reasonable requests.]

References

1. M. Allen, D. Tildesley, *Computer Simulation of Liquids* (Oxford Science, London, 1990)
2. M.C. Payne, M.P. Teter, D.C. Allan, T.A. Arias, J.D. Joannopoulos, Rev. Mod. Phys. **64**, 1045 (1992)
3. D. Frenkel, B. Smit, *Understanding Molecular Simulation*, 2nd edn. (Academic Press, San Diego, 2002)
4. M. Karplus, J. McCammon, Nat. Struct. Mol. Biol. **9**(9), 646 (2002)
5. D.C. Rapaport, *The Art of Molecular Dynamics Simulation*, 2nd edn. (Cambridge University Press, Cambridge, 2004). https://doi.org/10.1017/CBO9780511816581

6. D. Marx, J. Hutter, *Ab Initio Molecular Dynamics: Basic Theory and Advanced Methods* (Cambridge University Press, Cambridge, 2009). https://doi.org/10.1017/CBO9780511609633
7. D. Perez, B.P. Uberuaga, Y. Shim, J.G. Amar, A.F. Voter, (Elsevier, 2009), pp. 79–98. https://doi.org/10.1016/S1574-1400(09)00504-0. http://www.sciencedirect.com/science/article/pii/S1574140009005040
8. M.E. Tuckerman, *Statistical Mechanics: Theory and Molecular Simulation* (Oxford University Press, New York, 2010)
9. B. Kirchner, J. di Dio Philipp, J. Hutter, Top. Curr. Chem. **307**, 109 (2012)
10. K. Kadau, T.C. Germann, P.S. Lomfahl, Int. J. Mod. Phys. C **17**(12), 1755 (2006). https://doi.org/10.1142/S0129183106010182
11. T.C. Germann, K. Kadau, Int. J. Mod. Phys. C **19**(09), 1315 (2008). https://doi.org/10.1142/S0129183108012911
12. C.L. Brooks, D.A. Case, S. Plimpton, B. Roux, D. van der Spoel, E. Tajkhorshid, J. Chem. Phys. **154**(10), 100401 (2021). https://doi.org/10.1063/5.0045455
13. A.M.N. Niklasson, C.J. Tymczak, M. Challacombe, Phys. Rev. Lett. **97**, 123001 (2006)
14. A.M.N. Niklasson, Phys. Rev. Lett. **100**, 123004 (2008)
15. P. Steneteg, I.A. Abrikosov, V. Weber, A.M.N. Niklasson, Phys. Rev. B **82**, 075110 (2010)
16. G. Zheng, A.M.N. Niklasson, M. Karplus, J. Chem. Phys. **135**, 044122 (2011)
17. M.J. Cawkwell, A.M.N. Niklasson, J. Chem. Phys. **137**, 134105 (2012)
18. J. Hutter, WIREs Comput. Mol. Sci. **2**, 604 (2012)
19. L. Lin, J. Lu, S. Shao, Entropy **16**, 110 (2014)
20. M. Arita, D.R. Bowler, T. Miyazaki, J. Chem. Theory Comput. **10**, 5419 (2014)
21. P. Souvatzis, A.M.N. Niklasson, J. Chem. Phys. **140**, 044117 (2014)
22. A.M.N. Niklasson, M. Cawkwell, J. Chem. Phys. **141**, 164123 (2014)
23. K. Nomura, P.E. Small, R.K. Kalia, A. Nakano, P. Vashista, Comput. Phys. Commun. **192**, 91 (2015)
24. A. Albaugh, O. Demardash, T. Head-Gordon, J. Chem. Phys. **143**, 174104 (2015)
25. C.F.A. Negre, S.M. Mnizsewski, M.J. Cawkwell, N. Bock, M.E. Wall, A.M.N. Niklasson, J. Chem. Theory Comput. **12**, 3063 (2016)
26. A.M.N. Niklasson, J. Chem. Phys. **147**, 054103 (2017)
27. J.A. Bjorgaard, D. Sheppard, S. Tretiak, A.M.N. Niklasson, J. Chem. Theory Comput. **14**(2), 799 (2018). https://doi.org/10.1021/acs.jctc.7b00857. PMID: 29316401
28. A.M.N. Niklasson, J. Chem. Phys. **152**, 104103 (2020)
29. A.M.N. Niklasson, J. Chem. Theory Comput. **16**, 3628 (2020)
30. A.M.N. Niklasson, J. Chem. Phys. **154**, 0000 (2021)
31. C.F.A. Negre, A.M.N. Niklasson, A. Redondo, *Quantum-Based Molecular Dynamics Simulations with Applications to Industrial Problems* (Springer International Publishing, Cham, 2021), pp. 289–314
32. A.M.N. Niklasson, P. Steneteg, N. Bock, J. Chem. Phys. **135**, 164111 (2011)
33. N. Goldman, L.E. Fried, J. Phys. Chem. C **116**(3), 2198 (2012). https://doi.org/10.1021/jp206768x
34. P. Souvatzis, A.M.N. Niklasson, J. Chem. Phys. **139**, 214102 (2013)
35. P. Souvatzis, Comput. Phys. Commun. **185**(1), 415 (2014). https://doi.org/10.1016/j.cpc.2013.09.014. https://www.sciencedirect.com/science/article/pii/S0010465513003159
36. PetaChem, LLC (2020). http://www.petachem.com/doc/userguide.pdf
37. B. Aradi, A.M.N. Niklasson, T. Frauenheim, J. Chem. Theory Comput. **11**, 3357 (2015)
38. V. Vitale, J. Dziezic, A. Albaugh, A. Niklasson, T.J. Head-Gordon, C.K. Skylaris, J. Chem. Phys. **12**, 124115 (2017)
39. L. Lagardere, L.H. Jolly, F. Lipparini, F. Aviat, B. Stamm, Z.F. Jing, M. Harger, H. Torabifard, G.A. Cisneros, M.J. Schnieders, N. Gresh, Y. Maday, P.Y. Ren, J.W. Ponder, J.P. Piquemal, Chem. Sci. (2018). https://doi.org/10.1039/C7SC04531J
40. L.D.M. Peters, J. Kussmann, C. Ochsenfeld, J. Chem. Theory Comput. **13**, 5479 (2015)
41. T. Otsuka, M. Taiji, D.R. Bowler, T. Miyazaki, Jpn. J. Appl. Phys. **55**(11), 1102B1 (2016). http://stacks.iop.org/1347-4065/55/i=11/a=1102B1
42. T. Hirakawa, T. suzuki, D.R. Bowler, T. Myazaki, J. Phys. Condens. Matter **29**, 405901 (2017)
43. A. Albaugh, A.M.N. Niklasson, T. Head-Gordon, J. Phys. Chem. Lett. **8**, 1714 (2017)
44. A. Albaugh, T. Head-Gordon, J. Chem. Theory Comput. **13**, 5207 (2017)
45. A. Albaugh, T. Head-Gordon, A.M.N. Niklasson, J. Chem. Theory Comput. **14**(2), 499 (2018). https://doi.org/10.1021/acs.jctc.7b01041. PMID: 29316388
46. P. Henning, A.M.N. Niklasson, Shadow Lagrangian dynamics for superfluidity. Kinet Relat Models **14**(2), 303–321 (2021)
47. M.P. Kroonblawd, R.K. Lindsey, N. Goldman, Chem. Sci. **10**, 6091 (2019)
48. M.P. Kroonblawd, N. Goldman, *Free Energies of Reaction for Aqueous Glycine Condensation Chemistry at Extreme Temperatures* (Wiley, New York, 2020), p. 271
49. G. Zhou, B. Nebgen, N. Lubbers, W. Malone, A.M.N. Niklasson, S. Tretiak, J. Chem. Theory Comput. **16**(8), 4951 (2020). https://doi.org/10.1021/acs.jctc.0c00243. PMID: 32609513
50. R. Car, M. Parrinello, Phys. Rev. Lett. **55**, 2471 (1985)
51. D.K. Remler, P.A. Madden, Mol. Phys. **70**, 921 (1990)
52. G. Pastore, E. Smargassi, F. Buda, Phys. Rev. A **44**, 6334 (1991)
53. F.A. Bornemann, C. Schütte, Numer. Math. **78**, 359 (1998)
54. D. Marx, J. Hutter, *Modern Methods and Algorithms of Quantum Chemistry* (ed. J. Grotendorst, John von Neumann Institute for Computing, Jülich, Germany, 2000), 2nd edn
55. M.E. Tuckerman, J. Phys. Condens. Matter **14**, 1297 (2002)
56. G. Zerah, J.J. Clerouin, E.L. Pollock, Phys. Rev. Lett. **69**, 446 (1992)
57. J.J. Clerouin, G. Zerah, E.L. Pollock, Phys. Rev. A **46**, 5130 (1992)

58. F. Lambert, J. Clerouin, S. Mazevet, Eur. Phys. Lett. **75**, 681 (2006)
59. M. Sprik, M.L. Klein, J. Chem. Phys. **89**(12), 7556 (1988). https://doi.org/10.1063/1.455722
60. M. Sprik, J. Chem. Phys. **95**, 2283 (1990)
61. D. Van Belle, M. Froeyen, G. Lippens, S.J. Wodak, Mol. Phys. **77**, 239 (1992)
62. G. Lamoureux, B.T. Roux, J. Chem. Phys. **119**, 3025 (2003)
63. B. Hartke, E. Carter, Chem. Phys. Lett. **189**, 358 (1992)
64. H.B. Schlegel, J.M. Millam, S.S. Iyengar, G.A. Voth, A.D. Daniels, G. Scusseria, M.J. Frisch, J. Chem. Phys. **114**, 9758 (2001)
65. S.S. Iyengar, H.B. Schlegel, J.M. Millam, G.A. Voth, G. Scusseria, M.J. Frisch, J. Chem. Phys. **115**, 10291 (2001)
66. J.M. Herbert, M. Head-Gordon, J. Chem. Phys. **121**, 11542 (2004)
67. J. Li, C. Haycraft, S.S. Iyengar, J. Chem. Theory Comput. **12**, 2493 (2016)
68. W. Heitler, F. London, Z. Phys. **44**, 455 (1927)
69. M. Born, R. Oppenheimer, Ann. Phys. **389**, 475 (1927)
70. P. Pulay, G. Fogarasi, Chem. Phys. Lett. **386**, 272 (2004)
71. I.S.Y. Wang, M. Karplus, J. Am. Chem. Soc. **95**, 8160 (1973)
72. A. Warshel, M. Karplus, Chem. Phys. Lett. **32**, 11 (1975)
73. C. Leforestier, J. Chem. Phys. **68**(10), 4406 (1978). https://doi.org/10.1063/1.435520
74. R.N. Barnett, U. Landman, Phys. Rev. B **48**, 2081 (1993)
75. G. Kresse, J. Hafner, Phys. Rev. B **47**, 558 (1993)
76. H.C. Andersen, J. Chem. Phys. **72**, 2384 (1980)
77. M. Parrinello, A. Rahman, Phys. Rev. Lett. **45**, 1196 (1980)
78. S. Nose, J. Chem. Phys. **81**, 511 (1984)
79. T. Arias, M. Payne, J. Joannopoulos, Phys. Rev. Lett. **69**, 1077 (1992)
80. J. Herbert, M. Head-Gordon, Phys. Chem. Chem. Phys. **7**, 3269 (2005)
81. T.D. Kühne, M. Krack, F.R. Mohamed, M. Parrinello, Phys. Rev. Lett. **98**, 066401 (2007)
82. J. Fang, X. Gao, H. Song, H. Wang, J. Chem. Phys **144**, 244103 (2016)
83. A.M.N. Niklasson, C.J. Tymczak, M. Challacombe, J. Chem. Phys. **126**, 144103 (2007)
84. A.M.N. Niklasson, P. Steneteg, A. Odell, N. Bock, M. Challacombe, C.J. Tymczak, E. Holmstrom, G. Zheng, V. Weber, J. Chem. Phys. **130**, 214109 (2009)
85. A.M.N. Niklasson, M.J. Cawkwell, Phys. Rev. B **86**, 174308 (2012)
86. P. Hohenberg, W. Kohn, Phys. Rev. B **136**, 864 (1964)
87. R.G. Parr, W. Yang, *Density-Functional Theory of Atoms and Molecules* (Oxford University Press, Oxford, 1989)
88. R. Dreizler, K. Gross, *Density-Functional Theory* (Springer, Berlin, 1990)
89. J.P. Channel, C. Scovel, Nonlinearity **3**, 231 (1990)
90. R. McLachlan, P. Atela, Nonlinearity **5**, 541 (1992)
91. B.J. Leimkuhler, R.D. Skeel, J. Comput. Phys. **112**, 117 (1994)
92. G.J. Martyna, M. Tuckerman, J. Chem. Phys. **102**, 8071 (1995)
93. B. Leimkuhler, S. Reich, *Simulating Hamiltonian Dynamics* (Cambridge University Press, Cambridge, 2004)
94. S. Melchionna, J. Chem. Phys. **127**(4), 044108 (2007). https://doi.org/10.1063/1.2753496
95. N. Grønbech-Jensen, Mol. Phys. **118**(8), e1662506 (2020). https://doi.org/10.1080/00268976.2019.1662506
96. J. Finkelstein, C. Cheng, G. Fiorin, B. Seibold, N. Grønbech-Jensen, J. Chem. Phys. **153**(13), 134101 (2020)
97. J. Gans, D. Shalloway, Phys. Rev. E **61**, 4587 (2000). https://doi.org/10.1103/PhysRevE.61.4587
98. R.D. Engel, R.D. Skeel, M. Drees, J. Comput. Phys. **206**, 432 (2005)
99. S.D. Bond, B.J. Leimkuhler, *Molecular Dynamics and the Accuracy of Numerically Computed Averages* (Cambridge University Press, Cambridge, 2007)
100. A. Coretti, S. Bonella, G. Ciccotti, J. Chem. Phys. **149**, 191102 (2018)
101. S. Bonella, A. Coretti, R. Vuilleumier, G. Ciccotti, Phys. Chem. Chem. Phys. **22**, 10775 (2020). https://doi.org/10.1039/D0CP00163E
102. A. Coretti, L. Scalfi, C. Bacon, B. Rotenberg, R. Vuilleumier, G. Ciccotti, M. Salanne, S. Bonella, J. Chem. Phys. **152**(19), 194701 (2020). https://doi.org/10.1063/5.0007192
103. E. Martinez, M.J. Cawkwell, A.F. Voter, A.M.N. Niklasson, J. Chem. Phys. **142**, 1770 (2015)
104. A. Odell, A. Delin, B. Johansson, N. Bock, M. Challacombe, A.M.N. Niklasson, J. Chem. Phys. **131**, 244106 (2009)
105. A. Odell, A. Delin, B. Johansson, M.J. Cawkwell, A.M.N. Niklasson, J. Chem. Phys. **135**, 224105 (2011)
106. D. An, S.Y. Cheng, T. Head-Gordon, L. Lin, J. Lu. Convergence of stochastic-extended Lagrangian molecular dynamics method for polarizable force field simulation. J. Comput. Phys. **438**, 110338 (2021). https://doi.org/10.1016/j.jcp.2021.110338. https://www.sciencedirect.com/science/article/pii/S0021999121002333
107. J. Kolafa, J. Comput. Chem. **25**, 335 (2003)
108. I. Leven, T. Head-Gordon, Phys. Chem. Chem. Phys. **21**(34), 18652 (2019)
109. A.M.N. Niklasson, M. Challacombe, Phys. Rev. Lett. **92**, 193001 (2004)
110. A.M.N. Niklasson, M.J. Cawkwell, E.H. Rubensson, E. Rudberg, Phys. Rev. E **92**, 063301 (2015)
111. Y. Nishimoto, J. Chem. Phys. **146**, 084101 (2017)
112. C.G. Broyden, Math. Comput. **19**, 577 (1965)
113. D.G. Anderson, J. Assoc. Comput. Mach. **12**, 547 (1965)
114. P. Pulay, Chem. Phys. Lett. **73**(2), 393 (1980)
115. P. Pulay, J. Comput. Chem. **3**(4), 556 (1982)
116. Y. Saad, M.H. Schultz, SIAM J. Sci. Stat. Comput. **7**, 856 (1986)
117. D. Knoll, D. Keyes, J. Comput. Phys. **193**, 357 (2004)
118. W. Kohn, L.J. Sham, Phys. Rev. B **140**, A1133 (1965)
119. R. McWeeny, Rev. Mod. Phys. **32**, 335 (1960)
120. A. Szabo, N.S. Ostlund, *Modern Quantum Chemistry*, 1 revised edn. (Mc Graw-Hill Inc., New York, 1989)

121. T. Helgaker, P. Jorgensen, J. Olsen, *Molecular Electronic-Structure Theory*, 1st edn. (Wiley, New York, 2002)
122. N.D. Mermin, Ann. Phys. **21**, 99 (1963)
123. A.M.N. Niklasson, V. Weber, J. Chem. Phys. **127**, 064105 (2007)
124. A.M.N. Niklasson, J. Chem. Phys. **129**, 244107 (2008)
125. P. Pulay, Mol. Phys. **17**(2), 197 (1969)
126. H.B. Schlegel, Theor. Chem. Acc. **103**, 294 (2000)
127. J.M. Thijssen, *Computational Physics* (Cambridge University Press, Cambridge, 1999)
128. M.J.S. Dewar, W. Thiel, Theor. Chim. Acta **46**, 89 (1977)
129. M.J.S. Dewar, E.G. Zoebisch, E.F. Healy, J.J.P. Stewart, J. Am. Chem. Soc. **107**, 3902 (1985)
130. M. Elstner, D. Poresag, G. Jungnickel, J. Elsner, M. Haugk, T. Frauenheim, S. Suhai, G. Seifert, Phys. Rev. B **58**, 7260 (1998)
131. J.J.P. Stewart, J. Mol. Model. **19**, 1 (2013)
132. P.O. Dral, X. Wu, W. Thiel, J. Chem. Theory Comput. **15**, 1743 (2019)
133. C. Bannwarth, E. Caldeweyher, S. Ehlert, A.H. ans, P. Pracht, J. Seibert, S. Spicher, S. Grimme, WIREs Comput. Mol. Sci. **11**, 1 (2020)
134. W. Malone, B. Nebgen, A. White, Y. Zhang, H. Song, J.A. Bjorgaard, A.E. Sifain, B. Rodriguez-Hernandez, V.M. Freixas, S. Fernandez-Alberti, A.E. Roitberg, T.R. Nelson, S. Tretiak, J. Chem. Theory Comput. **16**(9), 5771 (2020). https://doi.org/10.1021/acs.jctc.0c00248. PMID: 32635739
135. A. Krishnapryian, P. Yang, A.M.N. Niklasson, M.J. Cawkwell, J. Chem. Theory Comput. **13**, 6191 (2017)
136. B. Hourahine et al., J. Chem. Phys. **152**, 124101 (2020)
137. J. Behler, M. Parrinello, Phys. Rev. Lett. **98**, 146401 (2007). https://doi.org/10.1103/PhysRevLett.98.146401
138. A.P. Bartók, M.C. Payne, R. Kondor, G. Csányi, Phys. Rev. Lett. **104**, 136403 (2010). https://doi.org/10.1103/PhysRevLett.104.136403
139. M. Rupp, A. Tkatchenko, K.R. Müller, O.A. von Lilienfeld, Phys. Rev. Lett. **108**, 058301 (2012). https://doi.org/10.1103/PhysRevLett.108.058301
140. R. Ramakrishnan, P.O. Dral, M. Rupp, O.A. von Lilienfeld, J. Chem. Theory Comput. **11**(5), 2087 (2015). https://doi.org/10.1021/acs.jctc.5b00099. PMID: 26574412
141. A. Thompson, L. Swiler, C. Trott, S. Foiles, G. Tucker, J. Comput. Phys. **285**, 316 (2015). https://doi.org/10.1016/j.jcp.2014.12.018. http://www.sciencedirect.com/science/article/pii/S0021999114008353
142. S.A. Ghasemi, A. Hofstetter, S. Saha, S. Goedecker, Phys. Rev. B **92**, 045131 (2015). https://doi.org/10.1103/PhysRevB.92.045131
143. L. Shen, J. Wu, W. Yang, J. Chem. Theory Comput. **12**(10), 4934 (2016). https://doi.org/10.1021/acs.jctc.6b00663. PMID: 27552235
144. J. Behler, J. Chem. Phys. **145**(17), 170901 (2016)
145. K.T. Schütt, F. Arbabzadah, S. Chmiela, K.R. Müller, A. Tkatchenko, Nat. Commun. **8**, 13890 (2017)
146. J. Han, L. Zhang, R. Car, E. Weinan, Commun. Comput. Phys. **23**(3), 629 (2018)
147. H. Li, C. Collins, M. Tanha, G.J. Gordon, D.J. Yaron, J. Chem. Theory Comput. **14**(11), 5764 (2018). https://doi.org/10.1021/acs.jctc.8b00873. PMID: 30351008
148. J.S. Smith, B.T. Nebgen, R. Zubatyuk, N. Lubbers, C. Devereux, K. Barros, S. Tretiak, O. Isayev, A.E. Roitberg, Nat. Commun. **8**, 13890 (2017)
149. F. Noé, A. Tkatchenko, K.R. Müller, C. Clementi, Annu. Rev. Phys. Chem. **71**(1), 361 (2020). https://doi.org/10.1146/annurev-physchem-042018-052331. PMID: 32092281
150. S. Dick, M. Fernandez-Serra, Nat. Commun. **11**, 3509 (2020)
151. Z. Qiao, M. Welborn, A. Anandkumar, F.R. Manby, T.F. Miller, J. Chem. Phys. **153**(12), 124111 (2020). https://doi.org/10.1063/5.0021955
152. W.A. Harrison, *Electronic Structure and the Properties Of Solids: The Physics of the Chemical Bond* (Dover, New York, 1980)
153. W.M.C. Foulkes, R. Haydock, Phys. Rev. B **39**, 12520 (1989)
154. D. Porezag, T. Frauenheim, T. Köhler, G. Seifert, R. Kaschner, Phys. Rev. B **51**, 12947 (1995). https://doi.org/10.1103/PhysRevB.51.12947
155. M.W. Finnis, A.T. Paxton, M. Methfessel, M. van Schilfgarde, Phys. Rev. Lett. **81**, 5149 (1998)
156. T. Frauenheim, G. Seifert, M. Elstner, Z. Hajnal, G. Jungnickel, D. Poresag, S. Suhai, R. Scholz, Phys. Stat. Sol. **217**, 41 (2000)
157. P. Koskinen, V. Mäkinen, Comput. Mater. Sci. **47**(1), 237 (2009). https://doi.org/10.1016/j.commatsci.2009.07.013
158. M. Gaus, Q. Cui, M. Elstner, J. Chem. Theory Comput. **7**, 931 (2011)
159. C. Bannwarth, S. Ehlert, S. Grimme, J. Chem. Theory Comput. **15**, 1652 (2018)
160. N. Goldman, B. Aradi, R.K. Lindsey, L.E. Fried, J. Chem. Theory Comput. **14**(5), 2652 (2018). https://doi.org/10.1021/acs.jctc.8b00165. PMID: 29614217
161. R.K. Lindsey, M.P. Kroonblawd, L.E. Fried, N. Goldman, *Force Matching Approaches to Extend Density Functional Theory to Large Time and Length Scales* (Springer International Publishing, Cham, 2019), pp. 71–93
162. M.J. Cawkwell, et al., LATTE. Los Alamos National Laboratory (LA- CC-10004) (2010). http://www.github.com/lanl/latte
163. F.J. Vesely, J. Comput. Phys. **24**, 361 (1977)
164. W.J. Mortier, S.K. Ghosh, S. Shankar, J. Am. Chem. Soc. **108**(15), 4315 (1986). https://doi.org/10.1021/ja00275a013
165. A.K. Rappe, W.A. Goddard III, J. Phys. Chem **95**(8), 3358 (1991)
166. S.W. Rick, S.J. Stuart, B.J. Berne, J. Chem. Phys. **101**, 6141 (1994)
167. T.A. Halgren, D. Wolfgang, Curr. Opin. Struct. Biol. **11**, 236 (2001)
168. G.A. Kaminski, H.A. Stern, B.J. Berne, R.A. Friesner, J. Phys. Chem. A **108**, 621 (2004)
169. P.E.M. Lopes, B. Roux, A.D.J. MacKerell, Theor. Chem. Acc. **124**, 11 (2009)
170. P. Cieplak, F.Y. Dupradeau, Y. Duan, J. Wang, J. Phys. Condens. Matter **21**, 333102 (2009)

171. S. Naserifar, D.J. Brooks, W.A. Goddard, V. Cvicek, J. Chem. Phys. **146**(12), 124117 (2017). https://doi.org/10.1063/1.4978891
172. Z. Jing, C. Liu, S.Y. Cheng, R. Qi, B.D. Walker, J.P. Piquemal, P. Ren, Ann. Rev. Biophys. **48**(1), 371 (2019). https://doi.org/10.1146/annurev-biophys-070317-033349. PMID: 30916997
173. T.W. Ko, J.A. Finkler, S. Goedecker, J. Behler, Nat. Commun. **12**, 398 (2021)
174. N. Bock, M. Challacombe, C.K. Gan, G. Henkelman, K. Nemeth, A.M.N. Niklasson, A. Odell, E. Schwegler, C.J. Tymczak, V. Weber, FreeON. Los Alamos National Laboratory (LA-CC 01-2; LA- CC-04-086), Copyright University of California (2008). http://www.nongnu.org/freeon/
175. M. Challacombe et al.MondoSCF v1.0α9. Los Alamos National Laboratory (LA-CC 01-2). Copyright University of California (2001). http://www.t12.lanl.gov/home/mchalla/
176. C.K. Skylaris, P.D. Haynes, A.A. Mostofi, M.C. Payne, J. Chem. Phys. **122**(8), 084119 (2005). https://doi.org/10.1063/1.1839852
177. D.R. Bowler, R. Choudhury, M.J. Gillan, T. Miyazaki, Phys. Stat. Sol. B **243**(5), 898 (2006)
178. T.R. Nelson, A.J. White, J.A. Bjorgaard, A.E. Sifain, Y. Zhang, B. Nebgen, S. Fernandez-Alberti, D. Mozyrsky, A.E. Roitberg, S. Tretiak, Chem. Rev. **120**(4), 2215 (2020). https://doi.org/10.1021/acs.chemrev.9b00447. PMID: 32040312
179. S. Goedecker, Rev. Mod. Phys. **71**, 1085 (1999)
180. D.R. Bowler, T. Miyazaki, Rep. Prog. Phys. **75**, 036503 (2012)
181. F. Mauri, G. Galli, Phys. Rev. B **50**, 4316 (1994)
182. F. Shimojo, R.K. Kalia, A. Nakano, P. Vashista, Phys. Rev. B **77**, 085103 (2008)
183. A.P. Horsfield, A.M. Bratkovsky, M. Fearn, D.G. Pettifor, M. Aoki, Phys. Rev. B **53**, 12694 (1996). https://doi.org/10.1103/PhysRevB.53.12694
184. E. Tsuchida, J. Phys. Condens. Matter **20**, 294212 (2008)
185. E.H. Rubensson, A.M.N. Niklasson, SIAM J. Sci. Comput. **36**, 148 (2014). arXiv:1302.7292
186. A.M.N. Niklasson, S.M. Mnizsewski, C.F.A. Negre, M.J. Cawkwell, P.J. Swart, J. Mohd-Yusof, T.C. Germann, M.E. Wall, N. Bock, E.H. Rubensson, H. Djidjev, J. Chem. Phys. **144**, 234101 (2016)